Journal of Magnetic Resonance **142,** 37–56 (2000)
Article ID jmre.1999.1915, available online at http://www.idealibrary.com on IDEAL®

Analysis of the Radial and Longitudinal Effect in a Double TE_{104} and a Single TE_{102} Rectangular Cavity

Milan Mazúr,*[,1] Marián Valko,* and Harry Morris†

**Department of Physical Chemistry, Faculty of Chemical Technology, Slovak Technical University, Radlinského 9, SK-812 37 Bratislava, Slovakia; and †School of Pharmacy and Chemistry, Liverpool John Moores University, Byrom Street, Liverpool L3 3AF, United Kingdom*

Received December 22, 1998; revised August 17, 1999

The response of the cavity to the rotation of a pointlike sample in the horizontal (*y*–*z*) plane passing through the center of the Bruker double TE_{104} and single TE_{102} rectangular cavities in concentric circles of radii $\rho = 0$, 1, 2, 3, 4, and 5 mm from the cavity center (radial effect) has been analyzed. The experimentally observed dependencies of the EPR signal intensity, I_{pp}, showed the following: (i) for $\rho = 0$ mm (a sample position in the cavity center), I_{pp} is independent of the angle of rotation; (ii) for $\rho = 1$, 2, and 3 mm, the I_{pp} dependence progressively changes from circular to oval; (iii) when the radius is further increased to $\rho = 4$ and 5 mm, the I_{pp} dependence changes dramatically, giving a figure eight shape. These experimental observations are in very good agreement with the theoretical calculations, in which the response is modeled using modified Cassinian curves, $K(\rho, \phi)$. Similar trends were observed for any position of the horizontal (*y*–*z*) plane at which the sample is situated along the vertical *x* axis of the cavity; however, the amplitude of the signal decreases with increase in the absolute value of the *x* coordinate, $|x|$. The variation in the signal amplitude along the cavity *x* axis (longitudinal effect) can be calculated theoretically using a modified sine-squared curve, $G(x)$. In general, the response of the cavity to a pointlike sample situated at any position, $P(\rho, \phi, x)$, can be represented as a product of the mentioned Cassinian curve, $K(\rho, \phi)$, and sine-squared curve, $G(x)$, giving for the signal intensity $I_{pp}(\rho, \phi, x) \propto K(\rho, \phi)G(x)$. The response to a large cylindrical sample which is concentrically situated on the cavity *x* axis can then be obtained by integrating the above product, $K(\rho, \phi)G(x)$, over the sample volume. The nonlinear radial effect may give rise to a serious source of systematic error in quantitative EPR spectroscopy and shows that accurate and precise positioning of the sample in the microwave cavity is essential.

Key Words: **quantitative EPR spectroscopy; radial effect; pointlike sample; circular sample.**

INTRODUCTION

The influence of the variation of the sample size, shape, and positioning within the microwave cavity on the peak-to-peak height of the EPR signal intensity, I_{pp}, has been analyzed by Poole (*1*), Casteleijn *et al.* (*2*), Hyde's group (*3*), Eaton's group (*4, 5*), Nagy and Plaček (*6*), Barklie and Sealy (*7*), and also our group (*8–13*). In all cases the authors concluded that the variation of these parameters could cause significant, serious errors in quantitative EPR measurements. This fact is generally valid for any arbitrary microwave cavity and applies to both single and double cavities.

Casteleijn and coworkers (*2*) recommended that the overall effect of inserting a cylindrical sample of radius *r* and length *L* in the microwave cavity could be considered as a combination of both the radial and the length effect. This may be sufficiently accurate for most users, but remains an incomplete analysis, because the radial effect has been usually evaluated only at $L = 0$ rather than integrated over *L* and the length effect has been usually evaluated only at $r = 0$ rather than at all *r* (*14*). Strictly speaking, such an analysis is only applicable to point- and linelike samples.

The effect of sample length, the longitudinal effect, is well discussed in the literature. For a pointlike sample moving along the vertical axis of the cavity, the EPR signal intensity, I_{pp}, shows a sine-squared dependence on the sample position (*1–13*). For movement of a linelike sample ($r \rightarrow 0$), a modified sine-squared dependence is observed which shows a plateau if the length of the sample is greater than that of the cavity (*9, 10, 12*). The radial effect has been precisely analyzed by Casteleijn *et al.* (*2*) using a small DPPH sample about 1 mm in length and by Nagy and Plaček (*6*) using a pointlike sample, a small crystal of the stable nitroxide radical TEMPOL less than 0.1 mm in size, which was rotated in the horizontal planes around the vertical axis of the cavity in concentric circles with various radii. The I_{pp} dependence on rotation angle and for the different radii was found to be a complicated function with a significant increase of the signal intensity when the sample approached the right–left side walls of the cavity and a decrease when the sample approached the front–back walls of the cavity. This phenomenon has been previously neglected in the literature. Nagy and Plaček (*6*) suggested that this unusual I_{pp} dependence was due to the high nonuniformity of the modulation field produced by the pair of Helmholz coils, which are mounted in the left and right side walls of the microwave

[1] To whom correspondence should be addressed. E-mail: mazur@cvt.stuba.sk.

1090-7807/00 $35.00

cavity. Their results were obtained with a Varian E-4 EPR spectrometer with a multipurpose E-231 rectangular cavity. Unfortunately, the theoretical calculations using a strict mathematical description based on the fundamental Maxwells' equations and the Biot–Savarts' law give poor agreement between the theoretical values and experimental data (*15*). Therefore, the experimental data were approximated by cubic splines. Together with known polynomial coefficients, the average value of the signal intensity of the sample can be calculated by integrating these splines over the sample shape and its position in the cavity (*6, 15*).

The existence of both the longitudinal and radial effect, which are both highly nonlinear, requires accurate and precise positioning of each sample in the microwave cavity as the principal, necessary, and imperative condition in quantitative EPR spectroscopy.

To our knowledge, experimental data of the radial dependence of I_{pp} values for a pointlike sample rotated around the vertical axis of the cavity have not been published for any Bruker rectangular cavity. The aim of this paper is to present in detail the original results of such a study for the Bruker double TE_{104} and single TE_{102} rectangular cavities. This involved the recording and analyzing of 1650 EPR spectra for complete mapping of the full cavity space for each microwave cavity and the construction of the original, empirical model. The sources of the principal errors in quantitative EPR spectroscopy caused by the radial effect nonlinearity are discussed.

Casteleijn and coworkers (*2*), Randolph (*14*), Nagy and Plaček (*6*), and also our group (*9, 10, 12*) suggest that the longitudinal and the radial effect could be independent of each other and thus fully separable. Under such conditions, the spatial, three-dimensional I_{pp} dependence can be calculated as a product of these two effects. Therefore, the second aim of the paper is to present experimental and theoretical proof of the above hypothesis. This involved the recording and analysis of over 6000 EPR spectra for the different positions of a pointlike sample and the circular samples (with various diameters) in both the double TE_{104} and single TE_{102} rectangular cavities.

EXPERIMENTAL

The samples were prepared and I_{pp} values recorded according to the procedures described in Refs. (*8–12*). A short recapitulation, with specific references to the preparation of a pointlike sample and the circular samples with various diameters, is given below.

Sample Preparation

A pair of identical pointlike samples (selected from five samples as described in Refs. (*9*), (*10*), and (*12*) was prepared by making linelike samples with the material column length approximately $L = 1.0$ mm and i.d. = 1.0 mm (the final volume of the material was always less than 1 mm^3) as follows: The original tube (o.d. $\cong$ 4 mm) containing the standard powdered strong pitch sample was opened under an inert atmosphere and the material reloaded into a thin-walled quartz EPR tube (i.d. = 1.0 mm, length $L_0 = 30$ mm, wall thickness, L_W, less than 0.1 mm), whose ends were closed by micro rubber stoppers. The following basic procedure was used for filling the sample tubes: The powdered material was poured into the sample tube, shaken, and pressed hard by a small piston. Additional material was added if necessary to give the desired sample length, $L = 1$ mm, which was checked with a magnifying lens. The material which adhered to the glass surface of the residual empty part of the filled sample tube during the filling process was removed as described in (*9*), and the samples were weighed. The experimental error (SD in percent) in the volume weight of the pointlike samples prepared by the above procedure was about 0.4% or less (*9*). Once filled and weighed, the material column was covered with a thin plastic disk, the length of the empty part of the sample tube was carefully shortened to approximately 2 mm, the residual free space was filled with cotton wool, and finally the tube end was closed with a micro rubber stopper. This sample preparation procedure removes effectively the "mechanical" inaccuracies associated with the sample tube meniscus.

Pairs of identical circular samples of diameter cd were prepared as follows: Five identical circles for each of the diameters cd = 1, 2, 3, 4, 5, 6, 7, 8, 9, and 10 mm were cut from polyethylene film (thickness about 0.1 mm) by special, accurate calibrated hollow punches and accurately weighed (Mettler, AE 200). The experimental error (SD in percent) of the weight of the five circles cut for the given diameter was 0.6% or less. All circles were placed in large Petri dishes whose volume was much greater than the total volume of all samples, covered, and together exposed to saturated vapors of the nitroxide spin label 4-hydroxy-2,2,6,6-tetramethylpiperidine-*N*-oxyl, TEMPOL (Aldrich), at the regulated temperature of 75°C in an electric furnace overnight.

Selection of Pairs of Identical Circular Samples

To obtain high accuracy and precision, the following method was used to select two samples from the five samples prepared. Because the material of circles, thickness of circles, spin label, and doping procedure were identical, sample weight is directly proportional to $(cd)^2$. The dependence of sample weight vs sample diameter, cd, was plotted and approximated by a quadratic polynomial function using regression analysis (correlation, $r = 0.99$). The pairs of identical circular samples for each given diameter were selected using the following criteria simultaneously: (i) From the five samples, pairs of samples were selected on the basis of the similarity of their weight. (ii) From these sets, the pair whose weight/diameter characteristics most closely represented the quadratic polynomial regression line for all of the diameters was selected.

Apparatus, Instrumental Parameters, and EPR Signal Intensity Expression

The X-band (~9.6 GHz) EPR spectra were recorded using a field-modulated CW Bruker ER 200 D-SRC with Aspect computer EPR spectrometer with the original double TE_{104} (ER 4105 DR) (the first cavity was defined as the front cavity) and single TE_{102} (ER 4102 ST) rectangular cavity (*16*). The resonant frequency of the microwave cavity was the following: (i) theoretically calculated from the cavity dimensions according to Ref. (*1*), p. 264, 9.573 GHz; (ii) given in the ER Series User's Manual (*16*), 9.6 GHz (nominal frequency); (iii) experimentally obtained without and with a variable-temperature double-wall quartz Dewar inside the cavity, 9.706 and 9.409 GHz, respectively. The unloaded quality factor, Q_u, of the resonator was approximately 6000. High-frequency modulation (100 kHz) was performed by two Helmholz coils of approximate diameter 24 mm mounted into the left and right side walls of the cavity. The distance between the planes of the modulation coils was about 17 mm. For comparison, the diameter of the Helmholz coils of the single TE_{102} rectangular cavity (E-231) of the Varian E-4 EPR spectrometer used in Ref. (*6*) was about 21 mm, and the distance between the planes of the modulation coils was approximately 16.5 mm. Instrumental parameters identical to those described in the previous papers (*8–12*) were used. The temperature of the EPR laboratory was 16°C and was kept constant using air conditioning. In all cases, the intensity of the EPR signal was characterized by the peak-to-peak height of the first-derivative EPR signal, I_{pp}. For the convenience of the analysis, all I_{pp} values were normalized to the interval $\langle 0, 1 \rangle$. Statistical evaluation of the data obtained was carried out according to standard statistical procedures.

ROTATION AND MOVEMENT OF THE SAMPLE IN THE RECTANGULAR CAVITY

The location of the origin and axis orientation of the microwave rectangular cavity based and linelike sample based perpendicular coordinate system as well as the definition and designation of the important sample-connected and cavity-connected points are given in Fig. 1 of Ref. (*9*). Only a short recapitulation with specific references to the insertion, rotation, and movement of a pointlike sample and the circular sample of variable diameter in the rectangular cavity is given below. The symbol abbreviations and *x*-axis orientation are the same as those used in Refs. (*8–12*) for compatibility.

Figure 1 shows the origin location and the *x*-axis orientation of the microwave rectangular cavity connected perpendicular (a) and cylindrical (b) coordinate system together with the definition and designation of the important cavity-connected points. For simplification, only one cavity (e.g., the first) of the double TE_{104} rectangular cavity is shown. The description of the second cavity and the single TE_{102} cavity is the same. The

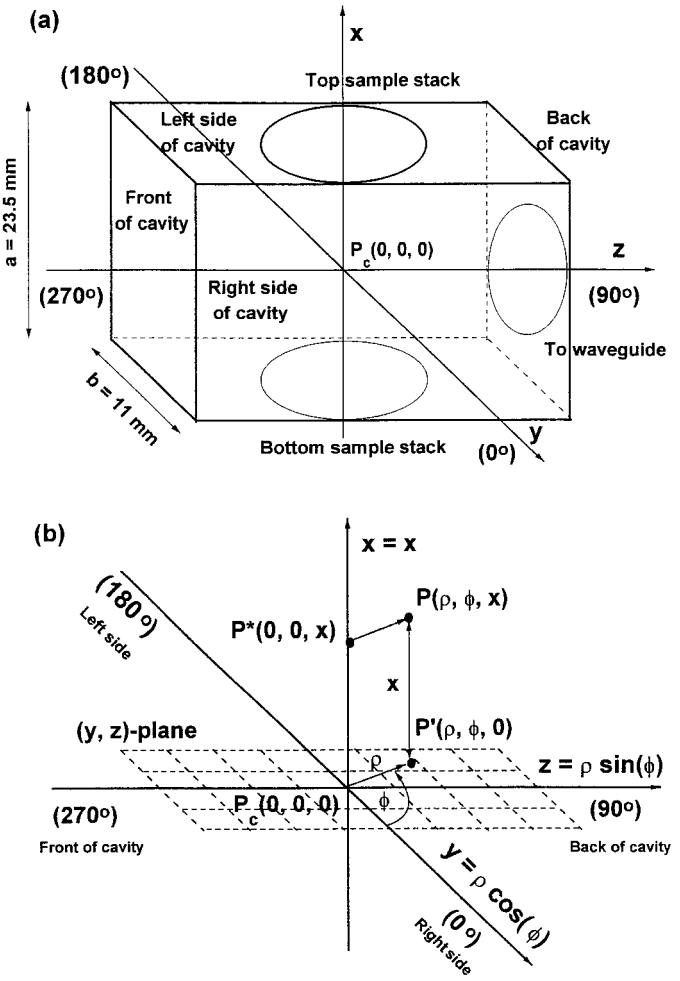

FIG. 1. Schematic diagram of the origin location and *x*-axis orientation of the perpendicular (a) and cylindrical (b) coordinate systems, and important points connected to the rectangular cavity. Definition of symbols used: *a*, depth of the microwave cavity ($a = 23.5$ mm), which is also the length of the active part of the cavity from the point of view of sample movement along the cavity *x* axis; *b*, width of the cavity ($b = 11$ mm), which is also the internal diameter of the top and bottom cylindrical access sample holes and the limit of the active part of the cavity from the point of view of sample rotation around the cavity *x* axis (i.e., the maximum radius of rotation of a pointlike sample, $\rho_{max} = b/2$), and also the maximum diameter of the circular sample; *d*, length of the cavity ($d = 42$ mm); $P_c(0, 0, 0)$, center of the cavity and location of the origin of both the rectangular and cylindrical coordinate systems. All the above data are valid for both the single TE_{102} and double TE_{104} Bruker rectangular cavities, except *d*, which is 2×42 mm for the double TE_{104} cavity. For comparison, the corresponding dimensions of the single TE_{102} rectangular cavity (E-231) of the Varian E-4 EPR spectrometer used in Ref. (*6*) were $a = 22.9$ mm, $b = 10.2$ mm, and $d = 25.4$ mm. (For further details, see text.)

definition of the cylindrical coordinate system is straightforward, except that (i) the polar axis coincides with the positive direction of the *y* axis and (ii) the *x* axes are the same in both coordinate systems. The symbols used in the cylindrical coordinate system have their usual meanings: ρ is the radius of the orbit of sample rotation, ϕ is the polar angle and also the angle of sample rotation, and *x* is the vertical position of the sample

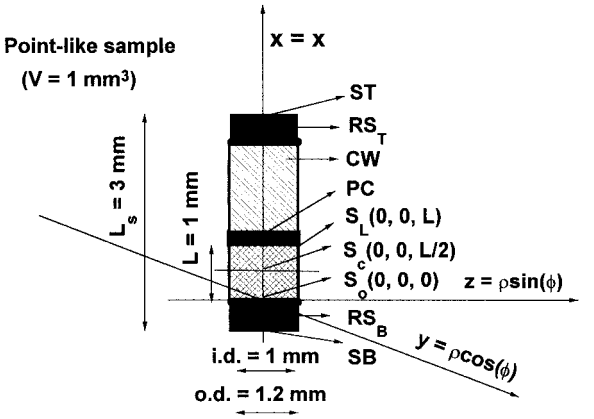

FIG. 2. Schematic diagram of the origin location and x-axis orientation of the perpendicular and cylindrical coordinate systems, and important points connected to a pointlike sample. Definition of symbols used: L_S, length of the sample tube (3 mm); L, sample length (1 mm); i.d., sample internal diameter (1 mm); $S_c(0, 0, L/2)$, center of the sample; $S_0(0, 0, 0)$, bottom of the sample, the origin of both perpendicular and cylindrical sample based coordinate systems; $S_L(0, 0, L)$, top of the sample; RS_T and RS_B, top and bottom rubber stoppers, respectively; CW, cotton wool; PC, plastic cover (≅0.1 mm thick); L_W, sample tube wall thickness (≅0.1 mm); o.d., outer diameter of the sample tube (1.2 mm); ST, sample top; SB, sample bottom.

center relative to the center of the cavity and also the x coordinate of the horizontal (y–z) plane in which the sample is rotated. The position of an arbitrary point, P, in the space may be defined by its x coordinate and by the polar coordinates, ρ and ϕ, of its projection P′ on the (y–z) plane. See Fig. 1b. The transformations from the cylindrical to the rectangular coordinate system are $y = \rho \sin(\phi)$, $z = \rho \cos(\phi)$, and $x = x$. To facilitate comparisons of the I_{pp} radial dependence for the Bruker double TE_{104} and single TE_{102} rectangular cavities with those of Nagy and Plaček (*6*) for the Varian E-231 cavity (*17*), the same assignment of the cavity sides to the polar angle, ϕ was used: viz., at the right side of the cavity, $\phi = 0°$, at the back of the cavity, $\phi = 90°$, at the left side of the cavity, $\phi = 180°$, and at the front of the cavity, $\phi = 270°$; see Fig. 1.

Figure 2 shows the origin location and the x-axis orientation of the pointlike sample connected perpendicular and cylindrical coordinate systems together with the definition and designation of the important sample-connected points.

The cavity width, $b = 11$ mm, internal diameter of a pointlike sample, i.d. = 1.0 mm, and sample tube wall thickness, $L_W \cong 0.1$ mm, limited the maximum radius available for the sample rotation to be $\rho_{max} = (b - \text{i.d.})/2 - L_W \cong 4.9$ mm. Since the internal sample diameter is 1 mm, the sample material elementary volumes are then situated in the cavity on a concentric orbit with radius ρ in the interval $\rho \in \langle \rho - \text{i.d.}/2, \rho + \text{i.d.}/2 \rangle$; i.e., ρ_{max} spans the interval $\langle 4.4, 5.4 \text{ mm} \rangle$. The experimentally observed I_{pp} value in the given orbital radius, ρ, is then an averaged value of partial contributions of the signal intensity from the radii interval $\langle \rho - 0.5, \rho + 0.5 \text{ mm} \rangle$. Note: for simplicity, the radius $\rho_{max} \cong 4.9$ mm is henceforth referred to as 5 mm radius.

The sample position at the cavity center is defined in both rectangular and cylindrical coordinate systems such that the center of the sample coincides with the center of the microwave cavity; viz., $S_c(0, 0, L/2) \equiv P_c(0, 0, 0)$.

Pointlike Sample Alignment Procedure

In the case of vertical movement and rotation of a pointlike sample, the alignment procedure (see Fig. 1 in Ref. (*8*)) was modified as follows: The thin-walled quartz tube E was removed. The EPR sample tube J was attached via connector K to the rod F with a calibrated micrometer screw as described in Ref. (*8*). However, see Fig. 3a; the special plastic flag with the millimeter scale is attached to J and centered using the vertical mark VM. A pointlike sample is positioned and accurately

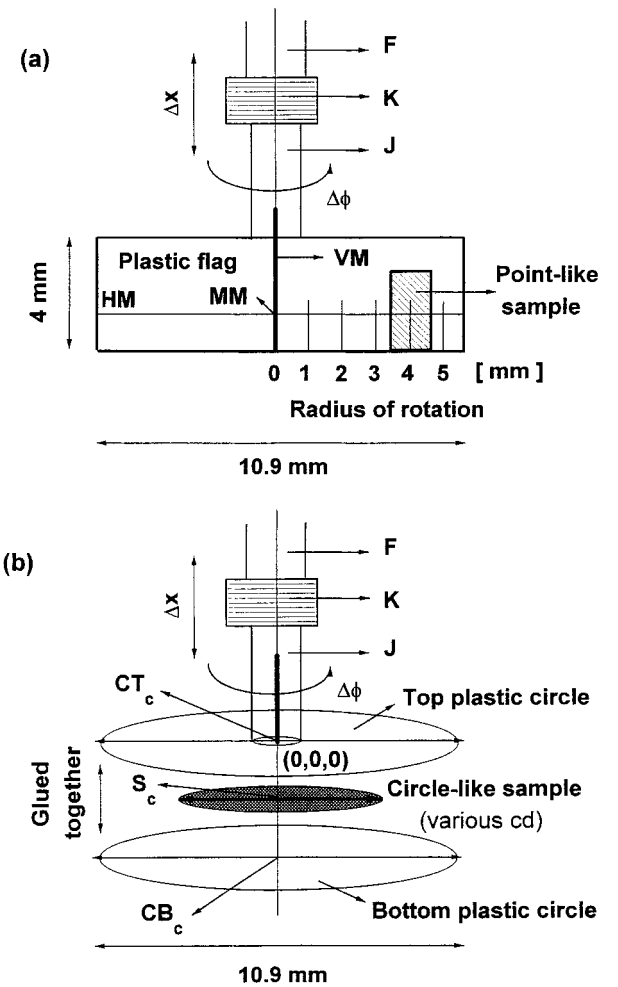

FIG. 3. Schematic diagram of the alignment procedure modified for (a) rotation of a pointlike sample on the orbits with various radii, ρ, around the cavity x axis; (b) movement of the circular samples with various diameters, cd, along the cavity x axis. (For symbol abbreviations and more information, see text).

glued (Duosan Rapid, Germany) to the plastic flag at the given orbital radius, ρ, with the sample center, $S_c(0, 0, L/2)$, coinciding with the horizontal mark HM and the appropriate radius mark on the millimeter scale. The final sample position was checked (to an accuracy of about 0.05 mm), and corrected if necessary, using a magnifying lens. The rod F was then attached to the goniometer micrometer sample rotator, and the plastic flag with a pointlike sample was inserted in the cavity central (y–z) plane using the modified alignment procedure given in Refs. (*8*), (*9*), and (*18*). The basic starting point of the sample rotation, $\phi = 0°$, was adjusted as follows: The zero point on the angular scale of the goniometer coincides with the positive direction of the y axis of the cavity and with the vertical plane of the plastic flag on the side where the sample is attached. The corrections to the outer diameter of a pointlike sample were included in the final position of the plastic flag. Anticlockwise rotation for a given radius, ρ, was performed in steps of 15° around a full circle $\phi \in \langle 0°, 2\pi \rangle$. After a full rotation, the values of $I_{pp}(\phi = 0°)$ and $I_{pp}(\phi = 360°)$ for any given radius were identical within experimental error. The I_{pp} values were also found to be independent of the starting point and of the direction (clockwise/anticlockwise) of rotation. This alignment procedure allowed the rotation of the sample in any given orbital radius, ρ, situated in a horizontal (y–z) plane perpendicular to the cavity x axis at any vertical position x. The accuracy of positioning of the sample is better than 0.1 mm for movement along the cavity x axis and 0.5° for rotation around the cavity x axis. The EPR signal intensity of the sample situated at 1650 different points within the microwave cavity was measured corresponding to 11 horizontal planes (with $x = 0, \pm 2.5, \pm 5.0, \pm 7.5, \pm 10.0$, and ± 12.0 mm) on 6 concentric circles (with $\rho = 0$, 1, 2, 3, 4, and 5 mm) in 15° intervals. The experimental data, $I_{pp}(\rho, \phi, x)$, for any one microwave cavity are stored in a cube matrix of $6 \times 25 \times 11$ elements.

Mapping of the Position, Rotation, and Vertical Movement of a Pointlike Sample in the Cavity

The case where $\rho = 0$, the position of a pointlike sample at the cavity center, is straightforward, $S_c(0, 0, L/2) \equiv P_c(0, 0, 0)$ (*1–13*). For the case where $\rho \neq 0$, the following accurate procedure for positioning the sample was used: The plastic flag with a pointlike sample situated at the given orbital radius, ρ, was inserted into the cavity and precisely positioned such that the point MM on the plastic flag (i.e., the intersection of the horizontal (HM) and vertical (VM) marks) coincided with the center of the cavity, $MM(0, 0, 0) \equiv P_c(0, 0, 0)$. The basic starting point of the sample rotation, $\phi = 0°$, was then adjusted as described above and fixed. Following this, the optimal vertical position of the sample center, corresponding to maximum EPR signal intensity, was maximum. This position was found experimentally by varying Δx and this point was again fixed. Such points on the x axis (with maximum values of I_{pp}) were found experimentally for all orbits of rotation, ρ, to be identically situated at the center of the cavity, $MM(0, 0, 0) \equiv P_c(0, 0, 0)$, which clearly demonstrated that all pointlike samples attached at different radii are situated in an identical (y–z) plane which is perpendicular to the cavity x axis and which crosses this axis at the cavity center, $P_c(0, 0, 0)$.

The definition and mapping for the movement of a pointlike sample along the cavity x axis have been fully analyzed and discussed (*9–13*). Here the x coordinate of the movement of a pointlike sample, $L = 1$ mm, along the cavity x axis is limited to $x \in \langle -(a + L)/2, (a + L)/2 \rangle$ although movement over this limit is possible but gives a zero EPR signal (*9, 10, 12*).

No differences were found for the first and second cavities of the double TE_{104} and single TE_{102} rectangular cavities.

Circular Sample Alignment Procedure

In the case of the circular sample movement, the above alignment procedure, seen in Fig. 3a, was modified as follows: The top plastic circle from the polypropylene film (circle diameter = 10.8 mm, thickness $\cong$ 0.1 mm) with central mark CT_c was concentrically and perpendicularly attached to the end of the sample tube J; see Fig. 3b. Following this, the circular sample from the polyethylene with variable diameter, cd, was concentrically glued (Duosan Rapid, Germany) to this circle, as $CT_c \equiv S_c$. Finally, the bottom plastic circle with central mark CB_c, identical to the top one, was again attached concentrically; thus $CT_c \equiv S_c \equiv CB_c$ was valid, and the microwave cavity was protected from contamination.

Mapping of Circular Sample Position and Movement in the Cavity

In this case the situation is much simpler because the rotation of the circular sample around the common sample–cavity x axis is not required (except to test the sample homogeneity). The sample position at the cavity center, $S_c(0, 0, L/2) \equiv P_c(0, 0, 0)$, is again straightforward. In principle, the circular sample with a variable diameter is the same as a cylindrical sample but with an extremely small length, $L = 0.1$ mm; therefore, a formalism identical to that introduced in Refs. (*9*), (*10*), and (*12*) can be used for the movement of the cylindrical sample along the common sample–cavity x axis. The circular sample movement along the x axis is again limited to $x \in \langle -(a + L)/2, (a + L)/2 \rangle$.

The circular sample was rotated around the common sample–cavity x axis and the I_{pp} dependence vs angle of rotation, ϕ, was investigated for all values of the sample diameter. In all cases, the I_{pp} was found to be independent of the angle ϕ, which illustrates that the samples are in fact homogeneous.

In the case of the circular sample with $L = 0.1$ mm, accurate positioning of the sample center at the point on the x axis at which the I_{pp} value was maximum is extremely important. These points with maximum I_{pp} values were found experimentally for all sample diameters, cd, to be identically situated in the center of the cavity, $S_c(0, 0, L/2) \equiv P_c(0, 0, 0)$. The

dependence of this sample central position on the circular sample diameter, cd, was not observed.

Again, no differences were found for the first and second cavities of the double TE_{104} and single TE_{102} rectangular cavities.

Discussion of the Material, Size, and Shape of the Samples Used

It is known that the spin-Hamiltonian parameters (g factor, hyperfine splitting, A, peak-to-peak linewidth, ΔH_{pp}, etc.) of paramagnetic centers in the single crystals are strongly dependent on the orientation of the crystal lattice axis in the microwave cavity (*19–23*), and the angular dependence of all these parameters on crystal rotation around its $\{x, y, z\}$ crystal lattice axis can be observed. To overcome the alignment problems associated with crystal anisotropy and the possible interference of these with the radial dependence of I_{pp}, a finely powdered material was chosen for a pointlike sample. A commercially available standard strong pitch sample consisting of 0.1% pitch dispersed in finely powdered solid KCl was used, so that the shape and area of its signal (a singlet) was independent of sample tube rotation around its axis. The experimentally determined spin-Hamiltonian parameters of the spectra of the strong pitch sample were identical to those reported in the literature (*1, 16, 22*) ($g_{eff} = 2.0028 \pm 0.0002$, $A_{eff} = 0.00$ G, $\Delta H_{pp} = 1.76 \pm 0.05$ G) and were found to be invariant of sample rotation around the cavity x axis on all orbits measured.

In the case of the circular sample with the various radii, it was clearly demonstrated that the experimentally observed EPR signal of the sample is itself averaged in the horizontal (y–z) plane, which removed any alignment problems associated with the anisotropy of the nitroxide spin label. The spin-Hamiltonian parameters of the EPR spectra of the stable nitroxide radical spin label, TEMPOL (*25, 26*), in the circular polyethylene sample were found to be the same for all measurements: viz., an axially symmetric ^{14}N triplet with $g_{\parallel} = 2.0027 \pm 0.0005$, $g_{\perp} = 2.0055 \pm 0.0005$, $A_{\parallel} = 34.95 \pm 0.05$ G, and $A_{\perp} = 13.44 \pm 0.05$ G. These accurate values of the spin-Hamiltonian parameters were determined using a standard sample (DPPH) and EPR spectra simulation (*27*) and are in the range commonly referred to in the literature for the nitroxide spin labels (*24–26, 28*). The experimental I_{pp} value was taken as the peak-to-peak height of the central peak ($m_I = 0$) of the triplet. The experimental spin-Hamiltonian parameters of TEMPOL and the I_{pp} values were found to be independent of the angle of rotation, provided the sample was accurately situated in a horizontal (y–z) plane.

The influence of the sample movement along the cavity x axis on the spin-Hamiltonian parameter values was analyzed and discussed in Refs. (*9*), (*10*), and (*12*). This phenomenon was carefully reverified for both a pointlike sample and the circular sample of all diameters, and the same results were obtained as reported in Refs. (*9*), (*10*), and (*12*); i.e., the spin-Hamiltonian parameters were invariant under movement of the sample along the cavity x axis.

In summary, the spin-Hamiltonian parameters of both (i) a strong pitch pointlike sample and (ii) circular samples of the nitroxide radical spin label TEMPOL were invariant under rotation around the cavity x axis and to movement along the cavity x axis.

The above-mentioned EPR experiments are based on the assumptions that (i) the perturbation of both microwave and modulation fields by the sample and sample holder is small and (ii) the sample material has small dielectric losses. The majority of solids fall into this category (*6*).

In practice, the optimum size and shape of the actual powdered pointlike sample used are limited by two opposing factors: (i) minimization of the microwave and modulation field perturbations, which is optimized using as small a sample size as possible, and (ii) maximization of the signal-to-noise ratio, which, in principle, requires as large a sample as possible. A suitable compromise was found using a small cylindrical sample ($L = 1$ mm, i.d. $= 1$ mm), which is similar in size to that used by Fajer and Marsh ($L = 1.5$ mm, o.d. $= 1.2$ mm) (*29*) and by Casteleijn *et al.* (L about 1 mm) (*2*). Casteleijn's group concluded that the deviation in the resonance frequency and power reflection factor of the cavity for such a sample were too small to be detectable. In the case of the circular samples, a constant thickness, 0.1 mm, of the doped polyethylene was found to be a suitable compromise.

Finally, identical thin-walled sample tubes for pointlike samples and identical materials for circular samples were used and the revised sample alignment setup components were examined both with an empty sample tube and with the undoped polyethylene circles; neither material displayed an EPR signal.

ANALYSIS OF VARIOUS EXPERIMENTAL SITUATIONS

The different combinations of possible experimental situations arising from the insertion and reinsertion of the sample, cavity retuning and remeasurement of spectra, and different starting points and different directions of sample movement along the common sample–cavity x axis in both double TE_{104} and single TE_{102} rectangular cavities were analyzed and discussed in Refs. (*9*), (*10*), and (*12*). These phenomena were carefully reverified for both the pointlike sample and circular sample, and the same trends of I_{pp} dependencies were observed as reported previously (*9, 10, 12*).

The rotation around the vertical cavity x axis of a circular sample of any diameter gives rise to an invariant I_{pp}. Consequently, the possible influence of sample reinsertion, cavity retuning, and remeasurement of spectra on I_{pp} during the experimental monitoring of the rotation of a pointlike sample in orbits of various radii, ρ, was analyzed. In each of the following cases, the sample was inserted at the starting point of the

rotation, the cavity was tuned, and the sample was rotated in steps of 15° and the spectra recorded.

(1) A pointlike sample was inserted into the cavity on a given orbital radius ρ at the different points with angles $\phi = 0°$ (at the right side of the cavity), 90° (at the back of the cavity), 180° (at the left side of the cavity), and 270° (at the front of the cavity). See Fig. 1 for comparison. The sample was then rotated from the starting point through 360° (i) anticlockwise (used as default rotation) and (ii) clockwise.

(2) Procedure 1 was repeated. However, the sample rotations in (1-i) and (1-ii) were performed from the starting points around to 90, 180, and 270° only, and then around to 720°.

(3) Procedures 1 and 2 were repeated. However, the sample was rotated around to the given target position and then back to the starting position using the reverse direction of the rotation.

(4) Procedures 1, 2, and 3 were again repeated. However, the sample was removed/reinserted and the cavity retuned at angles $\phi = 0$, 90, 180, 270, 360, and 720°.

The results of the above experiments clearly showed that the dependence of I_{pp} on the sample rotation was independent of the methods (1)–(4) by which it was measured.

As was summarized in Ref. (*18*), two series of sample movements are equivalent if they give an identical final position of the sample in the intercavity space and given an identical I_{pp} value, e.g., if the sample situated on the orbital radius, ρ, is (i) first rotated around the cavity x axis and then moved along the x axis and (ii) first moved along the x axis and then rotated around the x axis to the final sample position $P(\rho, \phi, x)$, in which $S_c(0, 0, L/2) \equiv P(\rho, \phi, x)$. See Ref. (*18*) for more details. Consequently, two sets of experiments were conducted and the results compared to verify this equivalency experimentally.

(a) The x coordinate of the (y–z) plane of the pointlike sample rotation was kept constant during the sample rotation around the cavity x axis to full circle in this (y–z) plane. Then the (y–z) plane was moved along the cavity x axis to the new position and the sample was again rotated around the cavity x axis to full circle.

(b) The angle of the pointlike sample rotation, ϕ, was kept constant and the sample was moved along the cavity x axis in the interval $x \in \langle -12, 12 \text{ mm} \rangle$. Then the sample was rotated around the cavity x axis to the new position and the sample was again moved along the x axis over the interval $x \in \langle -12, 12 \text{ mm} \rangle$.

The above experiments clearly showed that the trends of the I_{pp} dependencies obtained were unchanged if the sample was first rotated and then moved (a) or first moved and then rotated (b).

The same trends were observed whether the sample was in the first or second cavity of the double TE_{104} or in the single TE_{102} cavity. In addition, no observable differences were found if the complementary cavity of the TE_{104} contained a plastic flag (with or without an empty sample tube) or if it was completely empty. However, removal/reinsertion of a pointlike sample followed by retuning gave rise to a discontinuity in I_{pp} because the cavity was not identically biased. However, the trends remained the same and the effect could be corrected by a simple multiplicative factor. The I_{pp} values were also measured in the top and bottom sample access holes. However, all I_{pp} values in all sample rotation orbital radii, ρ, were observed to be zero within experimental error.

RESULTS AND DISCUSSION

Analysis of the Rotation of a Pointlike Sample in Various Orbital Radii around the Central x Axis of the Double TE_{104} and Single TE_{102} Rectangular Cavities

It is known that I_{pp} values depend strongly on the sample size, sample shape, and sample position within the microwave cavity (*1–13*) and that serious systematic errors may be incurred in quantitative EPR spectroscopy if cylindrical samples with different lengths and/or different internal diameters are compared. These sources of errors can be exacerbated by incorrect positioning of the sample in the microwave cavity. Consequently, the variation of I_{pp} values on the rotation of a pointlike sample around the cavity x axis for various orbital radii, ρ, and in various (y–z) planes perpendicular to the cavity x axis in the first and second cavities of the double TE_{104} rectangular cavity have been analyzed. The single TE_{102} rectangular cavity was used for comparison.

Figure 4 shows, in a polar coordinate system, how the normalized experimentally observed peak-to-peak height of the first-derivative EPR signal, I_{pp}, varies with anticlockwise rotation ($\phi \in \langle 0, 2\pi \rangle$) of a pointlike sample in the central (y–z) plane of the cavity (with $x = 0$ mm) on the orbits with radii, ρ, equal to 0, the sample position in the cavity center, 1, 2, 3, 4, and 5 mm around the x axis of the first cavity of the double TE_{104} rectangular cavity. Figure 4a corresponds to measurements in the empty cavity whereas Fig. 4b corresponds to equivalent measurements when the cavity contains a variable-temperature, double-wall quartz Dewar (in this case, the maximum radius is restricted to 3 mm). The I_{pp} value of a pointlike sample inserted in the center of the cavity, $P_c(0, 0, 0) \equiv S_c(0, 0, L/2)$, was independent of the rotation angle, ϕ, and therefore this value was taken as unity. The same trends of the I_{pp} dependencies were obtained for the second cavity of the double TE_{104} cavity and for the single TE_{102} rectangular cavity. The solid lines in Fig. 4 represent the modified Cassinian curves, which were theoretically computed according to an original empirical model (using Eq. [A14] of Appendix A). As with the experimental data, the theoretical I_{pp} was normalized for $\rho = 0$ mm. The agreement between theory and experiment is very good in all cases and any minor deviations can be attributed to the presence of the sample access holes (*7, 30*), to the possible

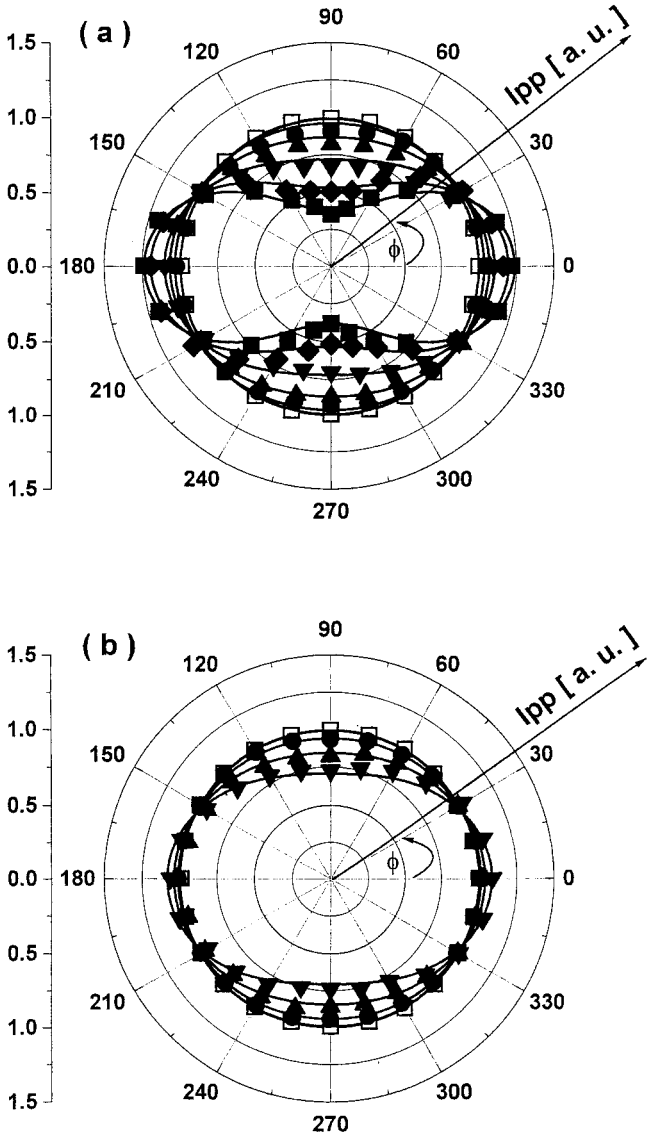

FIG. 4. Variation of the normalized experimentally observed peak-to-peak height of the first-derivative EPR signal, I_{pp}, with the anticlockwise rotation ($\phi \in \langle 0, 2\pi \rangle$) of a pointlike sample in the central (y–z) plane of the cavity on the orbits with radii ρ equal to 0 (□), 1 (●), 2 (▲), 3 (▼), 4 (◆), and 5 mm (■) around the x axis of the first cavity of the double TE_{104} rectangular cavity: (a) without and (b) with a variable-temperature quartz Dewar. The I_{pp} value of a pointlike sample inserted in the center of the cavity was taken as unity. The solid lines represent the modified Cassinian curves, which were theoretically computed according to an empirical model (using Eq. [A14]). The theoretical I_{pp} for $\rho = 0$ mm was taken as unity.

imperfection in the resonator shape (*6*, *15*), and to other possible nonuniformities in both the microwave and modulation fields (*1*, *6*, *7*), which were not included in the original empirical model. From Fig. 4, the following can be concluded:

(a) For the orbit with $\rho = 0$ mm (the cavity and sample centers are coincident), the experimental I_{pp} values show, within experimental error, no asymmetry and are independent of the sample rotation (SD of average value is 0.36% or less), in full accord with the previous published results (*9*, *10*). The experimental dependence can be modeled on the Cassinian curve, which for $\rho = 0$ mm is a circle. This illustrates that the sample is in fact homogeneous.

(b) For the orbits with $\rho = 1$, 2, and 3 mm, the radial dependence of experimental I_{pp} progressively changes from circular to oval with increasing radius of rotation, which again can be modeled on Cassinian curves.

(c) For $\rho = 4$ and 5 mm (in the real case $\rho \cong 4.9$ mm, because the thickness of the sample tube wall is about 0.1 mm or less), the shape of the experimental I_{pp} dependence changes dramatically. The oval is elongated in the left–right cavity direction and compressed in the front–back direction, giving a figure eight shape having maxima at $\phi = 0$ and 180° and minima at $\phi = 90$ and 270°. Again this behavior can be successfully modeled on Cassinian curves.

(d) All the experimental I_{pp} curves are symmetric both axially and with respect to the cavity center and intersect at four points: $K_1(\phi = 30°)$, $K_2(\phi = 150°)$, $K_3(\phi = 210°)$, and $K_4(\phi = 330°)$. This fact is again in very good agreement with the theoretical predictions using Cassinian curves and supports the validity of the approximation by the original empirical model.

(e) The presence of the variable-temperature, double-wall quartz Dewar (internal diameter slightly over 3 mm, wall thickness of the outer and inner quartz tubes 1 and 0.5 mm, respectively, and the vacuum gap between the two tubes about 1 mm) inserted inside the cavity did not affect the trends of the experimental I_{pp} dependencies. The "lens effect" of the quartz Dewar in the single TE_{102} rectangular cavity increased the I_{pp} amplitude compared to the case when the quartz Dewar was absent by the following factors: (i) for orbital radius $\rho = 0$ mm, 1.52 ± 0.01; (ii) for $\rho = 1$ mm, 1.47 ± 0.04; (iii) for $\rho = 2$ mm, 1.26 ± 0.04; and (iv) for $\rho = 3$ mm, 1.53 ± 0.03 (the averaged value from the full-circular I_{pp} dependence and SD of the averaged value). It is obvious that the lens effect is nonlinearly dependent on the orbital radius for reasons which are still unclear. The same trends were observed for the first and second cavities of the double TE_{104} cavity. However, the analysis of the lens effect in the first (the second) cavity of the double TE_{104} cavity. However, the analysis of the lens effect in the first (the second) cavity of the double TE_{104} rectangular cavity is much more complicated. In this case, the ratio $I_{pp,Dewar}/I_{pp,no\ Dewar}$ depends on the experimental configuration, i.e., whether an identical or different quartz Dewar is inserted in the complementary cavity or if this cavity is empty, because of the contribution of the field compression effect. Work is still continuing on this and related phenomena and will be the subject of a future paper.

(f) The coefficient of compression, the κ ratio (see Appendix B for definition), of the experimental and theoretical (shown in braces) curves in the central (y–z) plane (with $x = 0$ mm) of the double TE_{104} and single TE_{102} rectangular cavities

with and without the quartz Dewar are as follows: (i) for ρ = 0 mm, in the interval $\kappa \in \langle 0.99, 1.00\rangle$ and $\{1.00\}$; (ii) for orbital radius ρ = 1 mm, $\kappa \in \langle 0.89, 0.93\rangle$ and $\{0.93\}$; (iii) for ρ = 2 mm, $\kappa \in \langle 0.79, 0.82\rangle$ and $\{0.81\}$; (iv) for ρ = 3 mm, $\kappa \in \langle 0.60, 0.66\rangle$ and $\{0.65\}$; (v) for ρ = 4 mm, $\kappa \in \langle 0.43, 0.44\rangle$ and $\{0.44\}$; and (vi) for ρ = 5 mm, κ = 0.29 and $\{0.30\}$. The experimental and theoretical κ-ratio values are, within experimental error, the same.

(g) The values of $I_{pp}(\phi = 0°)$ and $I_{pp}(\phi = 360°)$ for any given radius of sample rotation were identical within the experimental errors (SD of average I_{pp} value was 0.30% or less).

(h) No significant differences were found between the first and second cavities of the double TE_{104} cavity and single TE_{102} rectangular cavity.

The theoretical analysis using the Cassinian model showed that (i) the boundary value of the radius, ρ, between the oval and figure eight shapes of the I_{pp} dependence was $\cong$3.4 mm, which is in good agreement with the experimental observation of ρ between 3 and 4 mm, and (ii) for the maximal radius of the "ideal" pointlike sample rotation, ρ_{max} = 5.5 mm, the calculated I_{pp} values of both minima of the figure eight were zero, and the Cassinian curve for ρ_{max} is a lemniscate. From the technical point of view, this boundary I_{pp} radial dependence, the lemniscate, is impossible to observe experimentally because of the finite size of the "real" pointlike sample. However, the trend of the experimental I_{pp} dependencies clearly approaches this theoretical limit with increasing ρ value from 4 to 5 mm.

The trends of the experimental I_{pp} dependencies observed in both the Bruker double TE_{104} and single TE_{102} rectangular cavities are very similar to those observed by Nagy and Plaček (*6*) in the Varian multipurpose E-231 rectangular cavity (of depth a = 22.9 mm and width b = 10.2 mm) in that when the sample approaches the right or left cavity side walls, a significant increase in I_{pp} values was observed, whereas when the sample approaches the front or back cavity walls, a significant decrease in I_{pp} was found. A possible explanation of this dependence could be the mutual effect of both the microwave and modulation fields. Possibly, the increase in I_{pp} value as the sample approaches the side walls can be attributed to the distance dependence of the magnetic field modulation amplitude. However, the decrease in moving toward the front and back wall is more likely to be dependent on variations in the microwave B_1 than on variation in modulation amplitude.

The experimental results and theoretical analysis clearly demonstrated that the dependence of the signal intensity, I_{pp}, on the rotation of a pointlike sample in the central (y–z) plane of the cavity around the cavity x axis on the various orbital radii, ρ, is a function of both polar variables, ρ and ϕ. Because this dependence is axially and cavity center symmetric, in principle, only the dependence in an arbitrary quadrant, e.g., the first one, could be studied. However, a slide asymmetry between some quadrants is apparent in the experimental data, and in praxis, the I_{pp} dependencies around to full circle must be verified. The experimental I_{pp} dependencies can be accurately approximated using Cassinian curves in which the cavity width, b = 11 mm, and the sample size (i.d. = 1 mm and $L_W \cong$ 0.1 mm) are the only parameters. This, in turn, limits the maximum radius of rotation, ρ_{max}, in the experiment. Thus the empirical model is clear and heuristic. See Appendix A for more details.

It is often assumed that the response in the (y–z) plane has $D_{\infty h}$ (circular) symmetry. Therefore, to estimate the magnitude/influence of the radial effect in quantitative EPR, further theoretical modeling was performed in which the oval and figure eight dependence of the signal intensity in the radial effect was ignored; i.e., the I_{pp} was assumed to be circular for all values of ρ. From a comparison of these two models, the following are evident:

(a) For ρ = 1 mm, the error introduced by incorrectly assuming a circular rather than an oval I_{pp} dependence is relatively small, but no negligible, with differences of 2.62% between the theoretically calculated I_{pp} values for these two models. However, for ρ = 2 and 3 mm, these differences rise very rapidly to 7.43 and 15.27%, respectively, giving rise to systematic errors in quantitative EPR if the oval dependence of the signal intensity in the radial effect is ignored. It should be noted that, in the case of a large cylindrical sample with i.d. = 4 mm, the sample lies within a radial ρ = 2 mm distance from the cavity center.

(b) If the figure eight dependence of the signal intensity in the radial effect is ignored, then for ρ = 4 and 5 mm, differences of 28.92 and 41.93%, respectively, are observed between the theoretically calculated I_{pp} values.

As mentioned previously, the movement of both pointlike and linelike samples along the common sample–cavity x axis (longitudinal effect) can be approximated by the theoretical curve calculated according to the modified sine-squared function (*1–11*). A better approximation can be achieved using the revised sine-squared curves calculated according to the integral equation [6] of Ref. (*12*). It was shown here that, for various orbital radii (radial effect), the rotation of a pointlike sample in the central (y–z) plane of the cavity (with x = 0 mm) around the cavity x axis can be approximated by modified Cassinian curves. Unfortunately, the longitudinal effect along the central x axis and the radial effect in the central (y–z) plane of the microwave cavity, i.e., at arbitrary points in the interactive space, are not exactly known. Consequently, the same variation obtained above for I_{pp} values on rotation of a pointlike sample around the cavity x axis for various orbital radii, ρ, was used. However, it was necessary to study the variation in the (y–z) planes with various x coordinates, $x \in \langle -12, 12$ mm$\rangle$, which are parallel with the central (y–z) plane of the cavity. For simplification of the notation, let the orbit with radius ρ (e.g., ρ = 2 mm) situated in the (y–z) plane with coordinate x (e.g.,

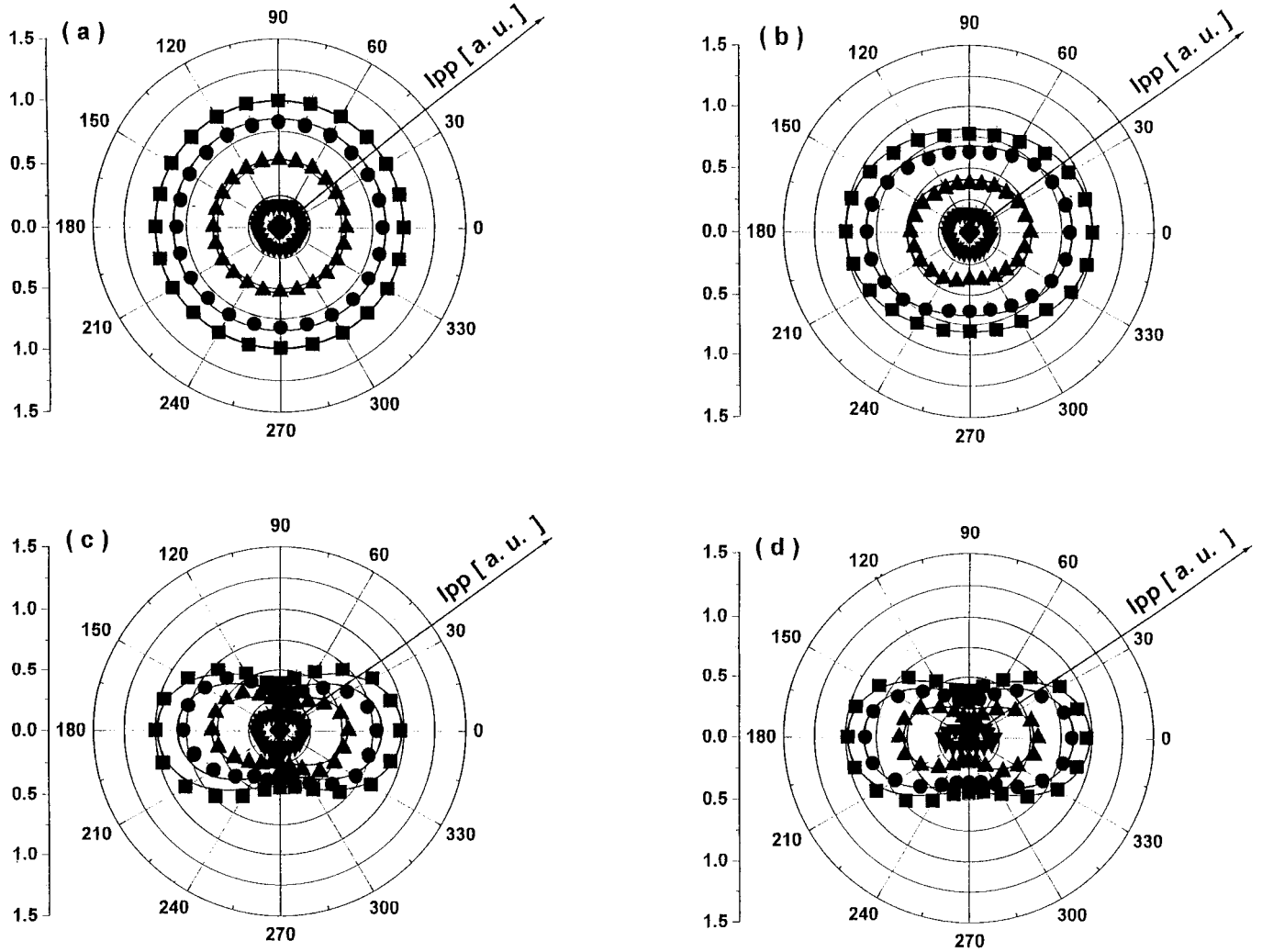

FIG. 5. Variation of the normalized experimentally observed peak-to-peak height of the first-derivative EPR signal, I_{pp}, with the anticlockwise rotation ($\phi \in \langle 0, 2\pi \rangle$) of a pointlike sample in the various (y–z) planes of the cavity around the x axis of the first cavity of the double TE_{104} rectangular cavity. The vertical coordinate of the (y–z) plane, x, is 0 (■), 2.5 (●), 5.0 (▲), 7.5 (▼), and 10 mm (◆) and the orbital radius is (a) $\rho = 0$ mm, (b) $\rho = 2$ mm, and (c) $\rho = 4$ mm. Plot d is the same as plot c except that the vertical coordinate, x, is 0 (■), −2.5 (●), −5.0 (▲), −7.5 (▼), and −10 mm (◆). The maximal I_{pp} value was taken as unity. The solid lines represent the theoretically computed curves using Eq. [A15]. As with the experimental data, the maximal I_{pp} value was taken as unity.

$x = 7.5$ mm) be indicated as the orbit with ($\rho = 2$ mm and $x = 7.5$ mm).

Figure 5 shows, in the polar coordinate system, how the normalized experimentally observed peak-to-peak height of the first-derivative EPR signal, I_{pp}, varied with anticlockwise rotation (polar angle, $\phi \in \langle 0, 2\pi \rangle$) of a pointlike sample in the various (y–z) planes of the cavity around the x axis of the first cavity of the double TE_{104} rectangular cavity. The vertical coordinate of the (y–z) plane, x, is 0 (the central (y–z) plane of the cavity), 2.5, 5.0, 7.5, and 10 mm, and the orbital radius is $\rho = 0$ mm (the sample position in the cavity center) (Fig. 5a). Figures 5b and 5c show the same information for orbital radii $\rho = 2$ mm and $\rho = 4$ mm, respectively, while, for comparison, Fig. 5d is the same as Fig. 5c except that the vertical movement of the sample is below the center of the cavity, −2.5, −5.0, −7.5, and −10 mm. The maximal I_{pp} value was again taken as unity. The I_{pp} values were found to be zero for $|x| \geq 12$ mm, giving no EPR signal in the sample access holes of the microwave cavity. The same trends of the I_{pp} dependencies were obtained for the second cavity of the double TE_{104} and single TE_{102} rectangular cavities. The solid lines in Fig. 5 represent the theoretically computed curves (using Eq. [A15]), which are the product of the corresponding Cassinian curves (calculated as above) and a "displacement" function (calculated from the single integration (numerical) of Eq. [A11] for the given vertical positions of the (y–z) plane after its movement along the cavity x axis. See Appendix A and Ref. (*12*) for further details. As with the experimental data, the maximal I_{pp} value was taken as unity. Again, the agreement between theory and experiment is very good in all cases and any minor deviations can be

attributed to the presence of the sample access holes (*7, 30*), the possible imperfection in the resonator shape (*6, 15*), and other possible nonuniformities of both the microwave and modulation fields (*1, 6, 7*), which were not included in the theoretical functions. From Fig. 5, the following can be concluded:

(a) For the orbit with $\rho = 0$ mm (the cavity and sample center were coincident), the experimental I_{pp} values show, within experimental error, no asymmetry and are independent of the sample rotation in the arbitrary (y–z) plane with vertical coordinate x in the interval $x \in \langle -10, 10 \text{ mm} \rangle$. (SD of average values was 0.37% or less for $x \in \langle -5, 5 \text{ mm} \rangle$ and between 1.68 and 2.12% for $|x| = 7.5$ mm; the signal-to-noise ratio increased slightly for $|x| = 10$ mm, giving an SD of 8.94–9.26%.) The amplitude of the I_{pp} values of the concentric circles decreased with increase in the absolute value of the x coordinate, $|x|$, according to the revised sine-squared curve (Eq. [A11]).

(b) For $\rho = 2$ mm and $x \in \langle -10, 10 \text{ mm} \rangle$, the radial dependencies of the experimental I_{pp} values change from a circular to oval form for all x values. The shape of these ovals does not change on the movement of the (y–z) plane of the sample rotation along the vertical x axis of the cavity, indicating that $I_{pp}(\rho, \phi, x)$ can, in practice, be factored into independent radial, $K(\rho, \phi)$, and displacement, $G(x)$, functions.

(c) For $\rho = 4$ mm and $x \in \langle -10, 10 \text{ mm} \rangle$, the experimental I_{pp} dependencies change from an oval to a figure eight for all x values. Here again, the shape was independent of the movement of the (y–z) plane along the cavity x axis and the effect of displacement along x can be modeled as above.

(d) No significant differences were found between the movement of the (y–z) plane in the positive (above the cavity center) and negative (below the cavity center) directions for any $x \in \langle -12, 12 \text{ mm} \rangle$ or between the first and second cavities of the double TE_{104} cavity and the single TE_{104} rectangular cavity. The presence of the variable-temperature quartz Dewar inside the cavity did not affect the trends of the experimental I_{pp} dependencies.

(e) The experimental and theoretical (given in braces), κ ratios of the I_{pp} dependencies in the various central (y–z) planes of the double TE_{104} and single TE_{102} cavities, with and without the quartz Dewar, were as follows: (i) for $\rho = 0$ mm and $x \in \langle -7.5, 7.5 \rangle$, $\kappa \in \langle 0.98, 1.00 \rangle$ and {1.00}; (ii) for $\rho = 2$ mm and $x \in \langle -7.5, 7.5 \rangle$, $\kappa \in \langle 0.76, 0.81 \rangle$ and {0.81}; and (iii) for $\rho = 4$ mm and $x \in \langle -7.5, 7.5 \rangle$, $\kappa \in \langle 0.42, 0.45 \rangle$ and {0.44}. Again, there is very good agreement between theory and experiment.

(f) $I_{pp}(\phi = 0°)$ and $I_{pp}(\phi = 360°)$ for given radius and in a given (y–z) plane of rotation were identical within the experimental errors (SD of average I_{pp} value was 0.30% or less).

If all experimental I_{pp} dependencies for a given orbital radius but various $|x|$ were normalized to unit amplitude, a very good visual and numerical match was obtained. All experimental curves are symmetric both axially and with respect to the cavity center and, within experimental error, no deformation of the I_{pp} curve shape was found as $|x|$ increased. This fact clearly demonstrated that the microwave cavity is very symmetrical and does not show any imperfections in the cavity shape.

In an earlier paper (*12*), the experimental dependencies of the EPR signal intensity on the movement of both pointlike and linelike samples along the central x axis of the cavity were correlated with the theoretical I_{pp} dependencies calculated according to (i) the modified sine-squared function and (ii) the integral equation [6] of Ref. (*12*). The results presented in this paper allow this to be generalized to any point within a cylindrical section of the cavity. This covers most of the experimental situations that arise in practice.

Figure 6 illustrates how the normalized experimentally observed peak-to-peak height of the first-derivative EPR signal, I_{pp}, varied with vertical movement, x, of the horizontal (y–z) plane of the cavity (in which a pointlike sample is rotated) along the cavity x axis and for the given angle of rotation ($\phi = 0°$ and $\phi = 90°$) on orbits with radii ρ equal to 0 (the sample position in the cavity center), 2, and 4 mm (Figs. 6a, 6b, and 6c, respectively) of the first cavity in the double TE_{104} rectangular cavity. Identical curves (within experimental error) were obtained for $\phi = 180°$ and $\phi = 270°$ (not shown). The data were extracted from Fig. 5. The maximal I_{pp} value was taken as unity. The same trends of the I_{pp} dependencies were obtained for the second cavity of the double TE_{104} cavity and for the single TE_{102} rectangular cavity. The solid lines in Fig. 6 represent the theoretically computed curves, which were calculated using the integral equation [A11]. The dashed lines were calculated using the modified sine-squared function (Eq. [A5]). Both theoretical displacement functions were calculated for the given vertical position of the linelike sample of small length, $L = 1$ mm, after its movement along the cavity x axis. See Refs. (*10*) and (*12*) for more details. The maximum value of the signal intensity was taken as unity. In both cases the agreement between theory and experiment is good. However, the theoretical predictions calculated with the revised sine-squared function (Eq. [A11]), which is slightly narrower, correlated better with the experimental data than those using the modified sine-squared function (Eq. [A5]). Note: According to Fig. 1a, the direction of ($\phi = 0°$ and $\phi = 180°$) is, in fact, the y axis of the cavity and the direction of ($\phi = 90°$ and $\phi = 270°$) is the z axis of the rectangular cavity. From Fig. 6, the following can be concluded:

(a) For $\rho = 0$ mm, the experimental I_{pp} values are independent of the sample rotation in the arbitrary (y–z) plane with the x coordinate (movement along the x axis) in the interval $x \in \langle -10, 10 \text{ mm} \rangle$. Therefore the I_{pp} values at $\phi = 0°$ (180°) and $\phi = 90°$ (270°) are identical, with coefficients of compression $\kappa = 1.00$. This is in full accord with the literature data (*9–11*).

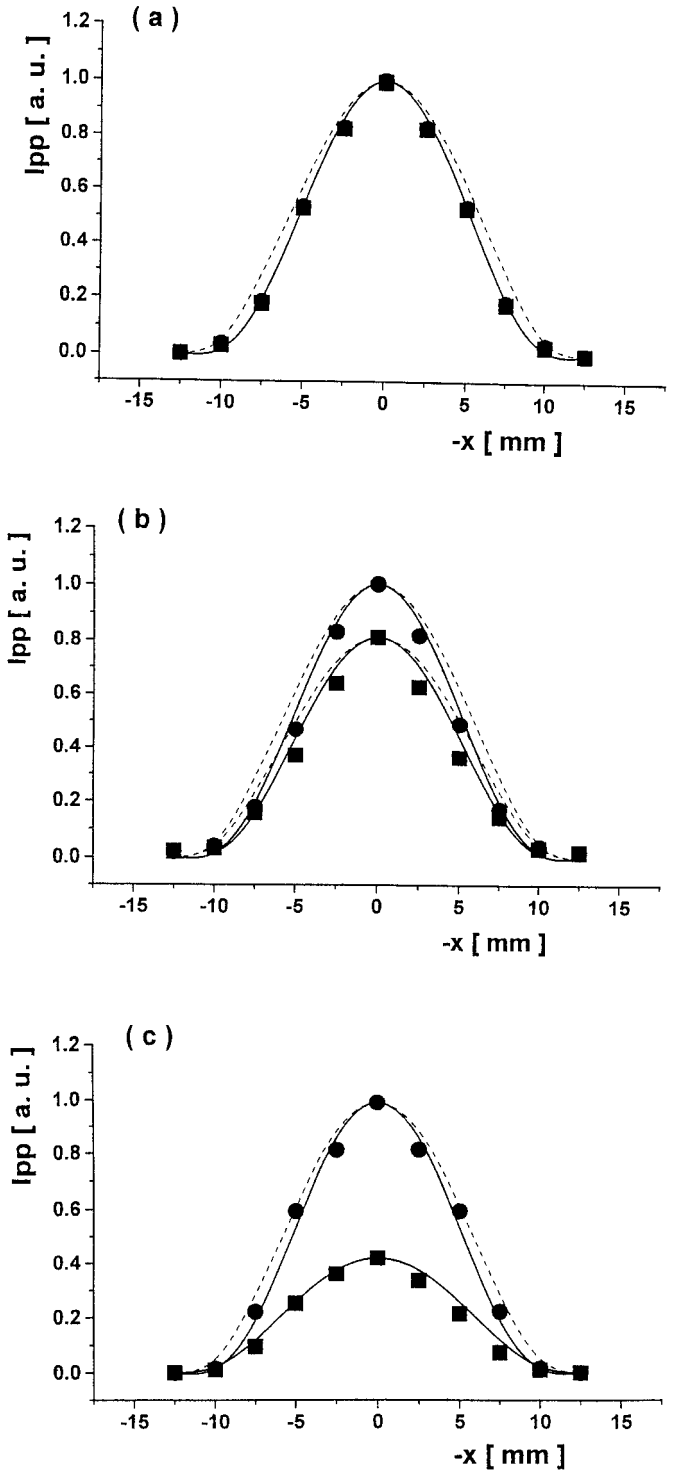

FIG. 6. Variation of the normalized experimentally observed peak-to-peak height of the first-derivative EPR signal, I_{pp}, with horizontal movement, x, of the horizontal (y–z) plane of the cavity (in which a pointlike sample is rotated) along the cavity x axis and for the given angle of rotation, $\phi = 0°$ (●) and $\phi = 90°$ (■), on orbits with radii ρ equal to (a) 0, (b) 2, and (c) 4 mm of the first cavity in the double TE_{104} rectangular cavity. the maximal I_{pp} value was taken as unity. The solid lines represent the theoretically computed curves calculated from the numerical integration of Eq. [A11]. The dashed lines represent equivalent theoretical curves calculated from the modified sine-squared function using Eq. [A5]. The maximum value of the signal intensity was taken as unity.

(b) For $\rho = 2$ mm, the I_{pp} dependencies are changed from circular to oval for all x coordinates. Therefore the I_{pp} values at $\phi = 0°$ (180°) are separated from the corresponding I_{pp} values at $\phi = 90°$ (270°), giving two pairs of curves with different amplitudes, the ratio of which is equal to the coefficient of compression $\kappa = 0.78$. All experimental I_{pp} dependencies are symmetric with respect to the central (y–z) plane of the cavity, and no significant differences were found between positive and negative movement of the sample along the cavity x axis.

(c) For $\rho = 4$ mm, the I_{pp} dependence is changed from oval to figure eight for all x coordinates. Therefore the I_{pp} values at $\phi = 0°$ (180°) are different from those at $\phi = 90°$ (270°), giving two pairs of dependencies whose amplitude ratio is equal to the coefficient of compression $\kappa = 0.43$.

In each of these cases a–c, the experimental dependence on x can be modeled as above. However, for case c there is a slight asymmetry in the experimental data as the x coordinate changes. The reason for this is unclear but is probably due to slight perturbations of both the microwave and modulation fields near the cavity walls.

(d) No significant differences were found between the first and second cavities of the double TE_{104} cavity and single TE_{102} rectangular cavity or when the quartz Dewar was present inside the cavity.

(e) The differences of the I_{pp} values between $\phi = 0°$ (180°) and also between $\phi = 90°$ (270°) were practically zero for $\rho = 0$ mm, and for $\rho = 2$ and 4 mm were within experimental error, but showed a slight increase with increase of both orbital radii and x coordinate.

Dependencies identical to those shown in Fig. 6 for another set of complementary pair of ϕ values (e.g., for $\phi = 60$ and 240° and for $\phi = 120$ and 300°) were also analyzed. The same trends as those shown in Fig. 6 were obtained.

The experimental data clearly demonstrated that (i) the movement of the sample rotation (y–z) plane along the x axis did not change the shape of the Cassinian curves and (ii) the decreasing values of the I_{pp} amplitude on the movement of the (y–z) plane can be accurately modeled on the revised sine-squared curves. Thus separation of the variables in a cylindrical coordinate system can be realized, and two independent effects—the radial effect, which is dependent only on the sample rotation in the (y–z) plane around the cavity x axis (i.e., on the polar coordinates ρ and ϕ), and the longitudinal effect, which is dependent only on sample movement along the x axis (i.e., on the coordinate x)—can be studied in the microwave cavity separately and independently of each other. See Appendix A for further details.

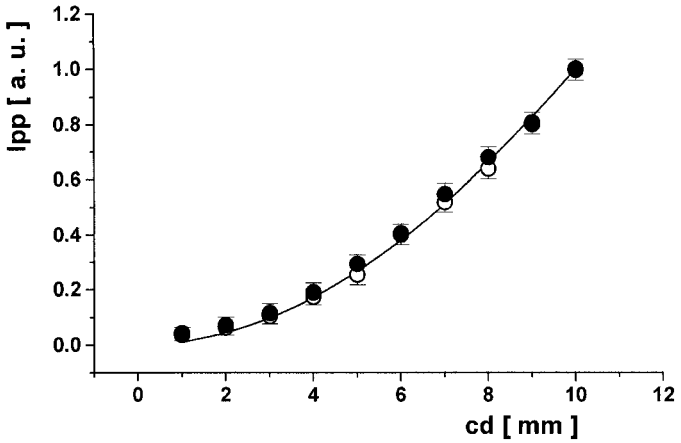

FIG. 7. Variation of the normalized experimentally observed peak-to-peak height of the first-derivative EPR signal, I_{pp}, with the diameter, cd $\in$ (1, 10 mm), of the circular sample situated in the central horizontal (y–z) plane in the first cavity of the double TE_{104} rectangular cavity (○) and in the single TE_{102} rectangular cavity (●). The averaged values are from five independent measurements. The maximal averaged I_{pp} value was taken as unity. The solid line represents the theoretically computed curve calculated from double integration (numerical) of the corresponding Cassinian curves (for the polar variables $\rho \in \langle 0, \text{cd}/2\rangle$ and $\phi \in \langle 0, 2\pi\rangle$) according to Eq. [A9]. Here again, the maximal I_{pp} value was taken as unity.

Analysis of Movement of Circular Samples of Various Diameters along the x Axis of the Double TE_{104} and Single TE_{102} Rectangular Cavities

It was shown herein that the radial effect could be approximated by the Cassinian curves in the central (y–z) plane of the cavity as well as in all planes parallel with this plane. To further investigate both the radial and longitudinal effects, the variation of I_{pp} for a series of circular samples of various diameters, cd, in various (y–z) planes perpendicular to the cavity x axis in the first and second cavities of the double TE_{104} rectangular cavity have been analyzed. The single TE_{102} rectangular cavity was again used for comparison.

Figure 7 shows how the normalized experimentally observed peak-to-peak height of the first-derivative EPR signal, I_{pp}, varied as a function of the diameter, cd $\in$ (1, 10 mm), of a circular sample situated in the central, horizontal (y–z) plane (i.e., with $x = 0$ mm and $S_c(0, 0, 0) \equiv P_c(0, 0, 0)$) in the first cavity of the double TE_{104} rectangular cavity and in the single TE_{102} rectangular cavity. In each case the averaged values are from five independent measurements. The maximal averaged I_{pp} value was taken as unity. The same trends of the I_{pp} dependencies were obtained for the second cavity of the double TE_{104} cavity. The solid line in Fig. 7 represents the theoretically computed curve calculated from double integration (numerical) of the corresponding Cassinian curves for the polar variables $\rho \in \langle 0, \text{cd}/2\rangle$ and $\phi \in \langle 0, 2\pi\rangle$ using Eq. [A9]. See Appendix A for more details. Again, as in the experimental case, the maximal I_{pp} value was taken as unity. The agreement between theory and experiment is very good and any slight differences, which are more apparent for small circular samples, can be attributed to the decrease in the signal-to-noise ratio of the I_{pp} values as the diameter of the samples decreased. The above agreement validates the use of a Cassinian model to represent the radial response of the cavity in the (y–z) plane.

To the best of our knowledge, there are neither experimental data nor theoretical calculations in the literature dealing with the movement of circular samples with variable diameters along the cavity x axis. Therefore, the dependence of I_{pp} values on both the x coordinate and circular sample diameter was investigated.

Figure 8 shows how the normalized experimentally observed peak-to-peak height of the first-derivative EPR signal, I_{pp}, varied as the circular sample, which is situated in the horizontal (y–z) plane of the cavity, was moved along the cavity x axis. The diameters of the samples are 10, 9, 8, 7, 6, 5, 4, 3, 2, and 1 mm in the first cavity of the double TE_{104} rectangular cavity

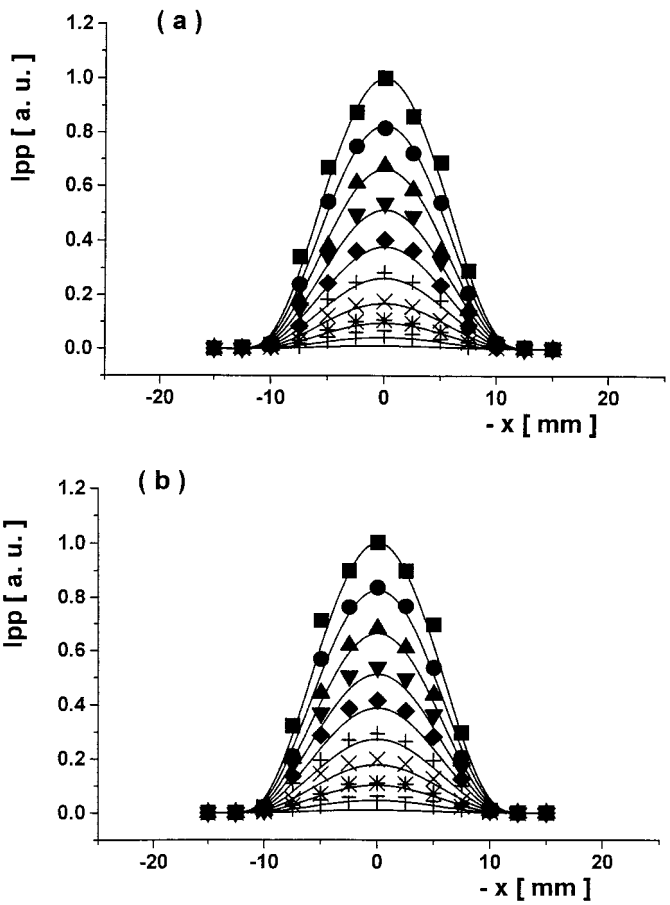

FIG. 8. Variation of the normalized experimentally observed peak-to-peak height of the first-derivative EPR signal, I_{pp}, with vertical movement, x, of the circular sample along the cavity x axis. The diameters, cd, of the samples are 10 (■), 9 (●), 8 (▲), 7 (▼), 6 (◆), 5 (+), 4 (×), 3 (*), 2 (—), and 1 mm (|) in the first cavity of the double TE_{104} rectangular cavity (a) and in the single TE_{102} rectangular cavity (b). The maximal I_{pp} value was again taken as unity. The solid lines represent the theoretically computed curves using Eq. [A8]. The maximal I_{pp} value was taken as unity.

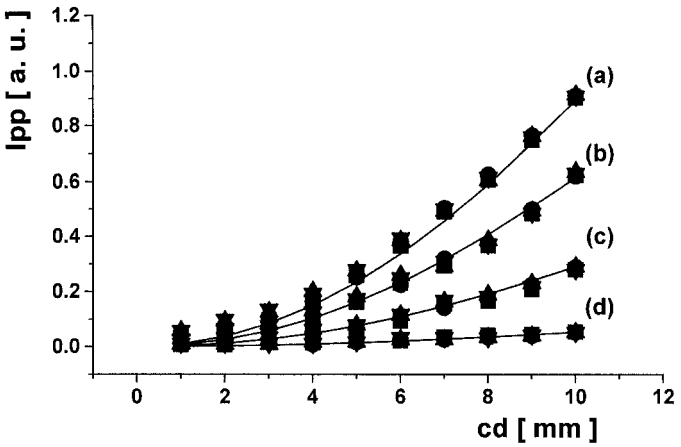

FIG. 9. Variation of the normalized experimentally observed peak-to-peak height of the first-derivative EPR signal, I_{pp}, with the diameter of the circular sample, cd $\in$ (1, 10 mm), and with the sample position in the cavity, x, equal to (a) ± 2.5, (b) ± 5, (c) ± 7.5, and (d) ± 10 mm in the first cavity of the double TE_{104} rectangular cavity (for positive (■) and negative (●) x values) and in the single TE_{102} rectangular cavity (for positive (▲) and negative (▼) x values). The maximal I_{pp} value for sample position in the center of the corresponding cavity was taken as unity. The solid lines represent the theoretically computed curves using Eq. [A8]. As with the experimental data, the maximal I_{pp} value for sample position in the cavity center was taken as unity.

(Fig. 8a) and in the single TE_{102} rectangular cavity (Fig. 8b). The maximal I_{pp} value was again taken as unity. The I_{pp} values were found to be zero for $|x| \geq 12$ mm (sample in the access holes). The same trends were obtained for the second cavity of the double TE_{104} rectangular cavity. The solid lines in Fig. 8 represent the theoretically computed curves (using Eq. [A8]), which are the product of the corresponding double integral (calculated as above) and a displacement function (calculated from the single integral (Eq. [A11]) for the given vertical positions of the circular sample after its movement along the cavity x axis). See Appendix A for more details. The maximal value was taken as unity. In all cases the agreement between theory and experiment is very good and any slight differences, which appeared for small circular samples, can be again attributed to the decrease in the signal-to-noise ratio of the I_{pp} values as the diameter of the samples decreased.

To precisely analyze the circular sample movement, a similar dependence as was shown in Fig. 7 was studied, but for various x coordinates (movement of the circular sample along the cavity x axis) in the interval $x \in \langle -10, 10 \text{ mm} \rangle$.

Figure 9 illustrates how the normalized experimentally observed peak-to-peak height of the first-derivative EPR signal, I_{pp}, varied with both the diameter of the circular sample, cd $\in$ (1, 10 mm), and its position in the cavity, x, equal to (a) ± 2.5, (b) ± 5, (c) ± 7.5, and (d) ± 10 mm (d) in the first cavity of the double TE_{104} rectangular cavity (for positive and negative x values) and in the single TE_{102} rectangular cavity (for positive and negative x values). The data were extracted from Fig. 8. The maximal I_{pp} value for sample position in the central (y–z) plane of the corresponding cavity was taken as unity. The same trends of the I_{pp} dependencies were obtained for the second cavity of the double TE_{104} cavity. The solid lines in Fig. 9 represent again the theoretically computed curves calculated as described above. As with the experimental data, the maximal I_{pp} value for sample position in the cavity center was taken as unity. The agreement between theory and experiment is very good and any slight differences can be attributed to the decrease in the signal-to-noise ratio as simultaneously $|x|$ is increased and sample diameter is decreased.

These results fully support the hypothesis that the radial and longitudinal effects are independent, and the separation of the corresponding variables in a cylindrical coordinate system is possible. Thus theoretical computation of the signal intensity of cylindrical samples of variable diameter and length can be performed as outlined in Appendix A.

It should be noted that the radial effect can only be approximated with a circular function for relatively small orbital radii, i.e., $\rho < 1$ mm, (which corresponds to the cylindrical sample of i.d. <1.5 mm), gives the systematic error of the I_{pp} values of 3% or less. However, for larger diameter tubes (EPR tubes of 3 mm and 4 mm i.d., which are commonly used in practice), has to be represented using the Cassinian curves, if not, then systematic errors of the I_{pp} values on the level about 10% or more are introduced.

To our knowledge, the precise and systematic analysis of the above mentioned phenomena and the importance of these error sources on the accuracy and reproducibility of the quantitative EPR spectroscopy has not been discussed in the literature and more attention to the investigation of these, and related phenomena will be needed in the future.

CONCLUSIONS

Radial effect. The experimentally observed dependence of signal intensity, I_{pp}, on the rotation of a pointlike sample in the horizontal (y–z) plane passing through the center of the single TE_{102} and double TE_{104} rectangular cavities in the concentric circles of rotation $\rho = 0$, 1, 2, 3, 4, and 5 mm around the cavity x axis showed the following: (i) for $\rho = 0$ mm (a sample positioned in the cavity center), I_{pp} is independent of the angle of rotation; (ii) for $\rho = 1$, 2, and 3 mm, the I_{pp} dependence progressively changes from circular to oval; (iii) when the radius is further increased to $\rho = 4$ and 5 mm, the I_{pp} dependence changes dramatically, and the oval is elongated in the left–right cavity direction and compressed in the front–back direction, giving a figure eight shape. This angular I_{pp} dependence can be modeled using the a modified Cassinian curve, $K(\rho, \phi)$.

Longitudinal effect. The angular I_{pp} dependence is independent of the movement of the horizontal (y–z) plane containing the sample from the center of the cavity along the cavity x axis. However, the amplitude of the signal decreased with increase in the absolute value of the x coordinate, $|x|$. This

variation in signal amplitude can be calculated theoretically using the modified/revised sine-squared curve, $G(x)$.

Combined radial and longitudinal effect. The experimentally observed dependence of I_{pp} on both (i) the rotation of a pointlike sample in the cavity (y–z) plane in orbits with various radii ρ around the x axis of the cavity and (ii) the movement of the sample rotation (y–z) plane along the cavity x axis can be accurately modeled by using the product of the corresponding Cassinian curve and sine-squared curve, $I_{pp}(\rho, \phi, x) \propto K(\rho, \phi)G(x)$.

Model verification. The experimentally observed dependence of the I_{pp} values on the movement of the circular sample of variable diameter along the cavity x axis can be theoretically computed as the product of the double integral of the corresponding Cassinian curves and single integral of the revised sine-squared function. The agreement between the theory and experiment is very good, which supports the validity of the empirical model.

These facts confirmed previous suggestions (see Refs. (*2*), (*6*), (*9–12*), and (*14*)) that the sample movement along the cavity x axis (longitudinal effect) and the sample rotation in the cavity (y–z) plane (radial effect) are independent of each other and can be fully separated.

The above-mentioned radial effect will give rise to serious sources of significant errors in quantitative EPR spectroscopy if the samples of identical material and identical length to be compared (i) have different diameters or (ii) have identical diameters but are situated at different sample positions in the cavity, off the cavity x axis. For the contribution of the longitudinal effect, see Refs. (*10*) and (*12*). Accurate and precise positioning of the sample in the microwave cavity is essential.

Finally, it should be noted that the results presented herein were obtained within a central cylinder of diameter 11 mm on an X-band, field-modulated CW Bruker ER 200 D-SRC EPR spectrometer with either a Bruker single TE_{102} or double TE_{104} rectangular cavity with the modulation coils situated in the left and right side cavity walls. Other EPR spectrometers which have different modulation facilities for different modulation frequencies could show greater or smaller differences than the results presented herein, and the given device and the experimental configuration used could be characterized with smaller or larger differences. The precise characteristics of the I_{pp} radial effect in a given microwave cavity are a necessary requirement in any quantitative EPR measurement.

APPENDIX A

I. Modeling of the Cavity Response to the Rotation of a Pointlike Sample

It is known that the intensity of the EPR signal of a pointlike sample is proportional to the product of the microwave magnetic field amplitude squared, $(H_1)^2$, and to the first power of the modulation field amplitude, H_m, at the sample position, and that both the microwave and modulation fields are highly nonuniform in the microwave cavity (*1–15*). Under these circumstances the I_{pp} dependence of a pointlike sample situated at any position in the cavity, normalized to the I_{pp} value of a pointlike sample at the cavity center, can be represented by the product $I_{pp}(y, z, x) \propto (H_1(y, z, x))^2 H_m(y, z, x)$. See Fig. 1 for definition of the cavity-based perpendicular coordinate system. In the present work, the response of such a sample situated at various positions in the cavity was determined experimentally. It was clearly shown that the I_{pp} values have cylindrical symmetry and that the linear, x, and radial, ρ and ϕ, variables could be treated independently. In earlier publications (*9–13*) it has been shown that the effect of the length and position on the central cavity axis on the I_{pp} of a linelike sample can be described in terms of parameters which were directly related to the cavity. The aim of the present paper is to extend this basic idea into the radial domain (i.e., devise an appropriate radial function which can describe the experimental data, within experimental error, and which is a function only of cavity-based parameters). To our knowledge, there is no such analytical expression in the literature. From an experimental point of view, the curves for the rotation of a pointlike sample in different circular orbits around the central cavity x axis have the following general properties: (1) the minimum symmetry is D_4 and the curves show a trend from circular, through oval, to a figure eight shape; (2) they have maxima at $\phi = 0$ and 180° and, above a certain radius $\rho \cong 3.4$ mm, minima at $\phi = 90$ and 270°; (3) for the angles $\phi = 30$, 150, 210, and 330°, the value of I_{pp} for a pointlike sample is approximately independent of the radius, ρ, and has a value of $\cong b$; and (4) the off-axis response at some points in the cavity (around $\phi = 0$ and 180°) is greater than at the center of the cavity.

Empirically, we have found that in the cylindrical coordinate system $\{\rho, \phi, x\}$ (see Fig. 1 for definition of the cavity-based cylindrical coordinate system), the radial function $K(\rho, \phi)$ can be accurately modeled with modified Cassinian curves (see Appendix B) of the form

$$K(\rho, \phi) = \sqrt{e^2\cos(2\phi) + \sqrt{b^4 - e^4\sin^2(2\phi)}} \quad [A1]$$

(in which only the plus sign is taken) and where $\phi \in \langle 0, 2\pi \rangle$, the empirical parameter b represents the practical width of the microwave cavity (11 mm for the Bruker TE_{102} and TE_{104} rectangular cavities) and the maximal possible radius of pointlike sample rotation $\rho_{max} = b/2$ (=5.5 mm), and the empirical parameter $e = 2\rho$ characterizes the rotation of a pointlike sample (with i.d. = 0 mm) on the circular orbit with radius $\rho \in \langle 0, b/2 \rangle$. Here the e parameter is equal directly to the diameter of the orbit. However, the sample used was not ideally pointlike, but has a real shape (a small cylinder with i.d. = 1 mm, $L = 1$ mm, and $L_W \cong 0.1$ mm). Therefore to correct for this, the parameter e is modified to $e = 2(\rho + \text{i.d.}/2)$, where $\rho \in \langle 0,$

$(b - \text{i.d.})/2 - L_W\rangle$, because here $\rho_{max} = (b - \text{i.d.})/2 - L_W$ ($\cong$4.9 mm). Thus the function is heuristic in the sense that it contains no arbitrary parameters. For definition and properties of the Cassinian curves, see Appendix B. Note: Since $b > 0$, $e \geq 0$, and $e \leq b$, $K(\rho, \phi)$ is always a real function. The sample rotation in the orbital radii $\rho > \rho_{max}$ is technically impossible for $\phi \in \langle 0, 2\pi\rangle$, because the cavity walls are the solid barrier.

It can be shown that the above function has the correct characteristic as outlined under 1–4 above. For example, at $\rho = 0$, for a pointlike sample (with i.d. = 0), $e = 0$, $K(0, \phi) = b$, and the shape is circular; at $0 < \rho \leq b/(2\sqrt{2})$, the shape is oval (the boundary oval for the Bruker TE_{102} and TE_{104} cavities is at $\rho \cong 3.9$ mm); at $b/(2\sqrt{2}) < \rho < b/2$, the shape is a figure eight, whereas at $\rho = b/2$, the shape is the lemniscate. In the case of a real pointlike sample (with i.d. = 1 mm), the mentioned correction must be taken into account. Then at $\rho = 0$, $e = 1$ and the $K(0, \phi)$ value is very slightly dependent on the sample rotation. However, the percentile SD of its over 2π averaged values is 0.29%, which is smaller that the experimentally obtained $I_{pp}(0, \phi)$ error bars (0.36%), and the very small differences between the circular $K(0, \phi)$ value and those calculated for a real pointlike sample can be neglected. At $0 < \rho \leq b/(2\sqrt{2}) - \text{i.d.}/2$, the shape is oval (the boundary oval for the Bruker TE_{102} and TE_{104} cavities now appears at $\rho \cong 3.4$ mm; cf. > 3.5 mm from experiment); at $b/(2\sqrt{2}) - \text{i.d.}/2 < \rho < b/2 - \text{i.d.}/2 - L_W$ ($\cong$4.9 mm), the shape is a figure eight. In the case of a real pointlike sample, $\rho_{max} < b/2$ and $e < b$ always. Therefore, it is impossible to obtain the shape of the Bernoulli lemniscate. The function has maxima at $\phi = 0$ and 180°, $K(\rho, 0°/180°) = \sqrt{(b^2 + (2\rho + \text{i.d.})^2)}$, which is greater than that at the center of the cavity, $\cong b$, and minima at $\phi = 90$ and 270°, $K(\rho, 90°/270°) = \sqrt{(b^2 - (2\rho + \text{i.d.})^2)}$, for $\rho \leq b/(2\sqrt{2}) - \text{i.d.}/2$, and finally at $\phi = 30$, 150, 210, and 330° cavity response is approximately independent of ρ with a value $\cong b$.

Comparison of values calculated with Eq. [A1] (correction of e parameter included) with the experimental data for the rotation of a real pointlike sample in the central (y–z) plane of the cavity for any value ρ and ϕ (see Fig. 4) shows that the function $K(\rho, \phi)$ predicts the I_{pp} angular response for all values within the experimental error. Furthermore, the experimental data show that the normalized I_{pp} for the sample in any plane parallel to the central (y–z) plane is the same. Therefore the above function can be applied to any arbitrary plane in the cavity.

II. Theoretical Calculation of the EPR Signal Intensity

It is known that the relative intensity of the EPR signal of a large homogeneous sample depends not only on the contents of the paramagnetic centers but also on the size and shape of the sample as well as its position and orientation in the given microwave cavity. See elsewhere (*1–12*). In the general case, the theoretical calculation of the EPR signal intensity, $I_{pp}(y, z, x)$, of the large sample is a three-dimensional problem, and the success of the solution is dependent on the size and shape of the large sample, on the position and orientation of the large sample in the cavity, on the type of the resonance mode of the microwave cavity, etc. The possible symmetry of the large sample and the adequate choosing of the coordinate system can considerably simplify the computation of the EPR signal intensity.

In the cylindrical coordinate system, $\{\rho, \phi, x\}$, then, from a practical point of view, the signal intensity, $I_{pp}(\rho, \phi, x)$, at any point due to the small volume element $\rho d\rho\, d\phi\, dx$ is given by

$$I_{pp}(\rho, \phi, x) \propto F(\rho, \phi, x)\rho d\rho\, d\phi\, dx. \qquad [A2]$$

The total signal intensity for a sample within the prescribed part of the cavity (a cylinder of diameter b running the full length of the cavity, a) can be obtained by integrating Eq. [A2] over the volume of the sample, D,

$$I_{pp}(D) \propto \iiint_D F(\rho, \phi, x)\rho d\rho\, d\phi\, dx. \qquad [A3]$$

The experimental data for the rotation of a pointlike sample in horizontal planes displaced above and below the central cavity x axis show that the normalized angular response is independent of the displacement. Therefore, $F(\rho, \phi, x)$ must be of the form

$$F(\rho, \phi, x) = G(x)\, K(\rho, \phi). \qquad [A4]$$

The function $G(x)$ represents the signal intensity of a pointlike sample displaced a distance x from the cavity center relative to that of the same sample at the cavity center. This is often approximated to a sine-squared function, or, without the $\pi/2$ shift, to a cosine-squared function (*1–7, 9–13*):

$$G(x) \propto \sin^2\left(\frac{\pi}{a}\left(x + \frac{a}{2}\right)\right) \propto \cos^2\left(\pi\frac{x}{a}\right). \qquad [A5]$$

Although this seems to work well with a pointlike sample, a more precise description is

$$G(x) \propto \frac{q_0 \cos^3\left(\pi\frac{x}{a}\right)}{\sqrt{1 + q_0^2 \cos^2\left(\pi\frac{x}{a}\right)}}, \qquad [A6]$$

where $a = 23.5$ mm for the Bruker TE_{102} and TE_{104} cavities.

See Refs. (*3*), (*12*), and (*13*) for more details. The function $K(\rho, \phi)$ was described above.

The displacement (Eqs. [A5] and [A6]) and radial (Eq. [A1]) functions can then be combined to give the EPR signal intensity for a sample situated at an arbitrary position within the X-band cavity:

$$I_{pp}(\mathrm{D}) \propto \iiint_{\mathrm{D}} \frac{q_0 \cos^3\left(\pi \frac{x}{a}\right)}{\sqrt{1 + q_0^2 \cos^2\left(\pi \frac{x}{a}\right)}} \times \sqrt{e^2 \cos(2\phi) + \sqrt{b^4 - e^4 \sin^2(2\phi)}}\ \rho d\rho\ d\phi\ dx. \quad [A7]$$

III. Special Cases

The solution of the above triple integral can be considerably simplified if the sample over whose shape the integration is performed has a regular cross section along at least one of its dimensions (e.g., circular cross section). In practice, the majority of the samples used in EPR fulfill the above conditions. It is further assumed that the sample shape can be described mathematically. A volume of revolution sample is typical of this sample shape, e.g., (i) a cylindrical sample with a circular cross section with a constant diameter or (ii) a sphere, ellipsoid of revolution, hyperboloid of revolution, parabaloid of revolution, etc. with a circular cross section with a variable diameter. Note: For a general shape of the sample, a shell method can be used.

1. Cylindrical Sample of Internal Diameter i.d. and Length L

1.1. Concentric situated on the central cavity x axis. In this case, which is widely used in EPR praxis, the x and $\{\rho, \phi\}$ variables can be easily separated and the triple integral, Eq. [A7], is reduced to a sequence of a single and a double integral:

$$I_{pp}(\mathrm{L_2}, \mathrm{L_1}, \mathrm{i.d.}) \propto \int_{L_1 \geq a/2}^{L_2 \leq a/2} \frac{q_0 \cos^3\left(\pi \frac{x}{a}\right)}{\sqrt{1 + q_0^2 \cos^2\left(\pi \frac{x}{a}\right)}}\, dx \int_0^{\mathrm{i.d.}/2} \int_0^{2\pi} \times \sqrt{4\rho^2 \cos(2\phi) + \sqrt{b^4 - 16\rho^4 \sin^2(2\phi)}}\ \rho d\rho\ d\phi, \quad [A8]$$

where the substitution $e = 2\rho$ was made, the upper and lower limits of integration along the x axis are $L_2 = {}^*L/2 + {}^*\mathrm{cc}$ and $L_1 = -{}^*L/2 + {}^*\mathrm{cc}$, respectively, and *cc is the distance between the cavity center, $\mathrm{P_c}(0, 0, 0)$, and the sample center, ${}^*\mathrm{S_c}(0, 0, {}^*L/2)$. The restrictions $L_2 \leq a/2$ and $L_1 \geq -a/2$ are applied to ensure that the integral only extends over that part of the cylindrical sample, $^*L$, which is really situated within the active part of the cavity, a. (It is always valid that $^*L \leq a$.) For calculation of $^*L$ and the *cc value when $L < a$, $L = a$, and $L > a$ and further detailed information, see Refs. (*12*) and (*13*). The restriction i.d. $\leq b - 2L_{\mathrm{W}}$ expresses the fact that the maximal available i.d. of the cylindrical sample is limited by the width of the cavity, b, and by the sample tube wall thickness, L_{W}.

Equation [A8] is valid for any position of the cylindrical sample which is concentrically situated on the cavity x axis. For the sample at the center of the cavity, $\mathrm{S_c}(0, 0, {}^*L/2) \equiv \mathrm{S_c}(0, 0, L/2) \equiv \mathrm{P_c}(0, 0, 0)$, $L_2 = {}^*L/2$ and $L_1 = -{}^*L/2$. Because of the symmetry of the integral over x and ϕ, it need only be integrated over the first octant, $x \in \langle 0, {}^*L/2\rangle$, $\phi \in \langle 0, \pi/2\rangle$, and multiplied by eight.

1.2. Movement of the cylindrical sample along the common sample–cavity x axis. In this case, the EPR signal intensity is computed using Eq. [A8] for each position of the cylindrical sample center, $\mathrm{S_c}(0, 0, L/2)$, during its movement along the common sample–cavity x axis, cc $\in \langle -(a + L)/2, (a + L)/2\rangle$, and the required profile of the signal intensity can be constructed from this set of I_{pp} values. The theoretical analysis and experimental investigation of this topic will be a subject of a future paper. Note: The double integral in Eq. [A8] has a constant value during the movement of the sample along the common sample–cavity x axis, because all cross sections of the cylindrical sample in any horizontal (y–z) plane of the cavity remain always circular with constant diameter i.d.

2. Circular Sample of Diameter cd and L → 0

2.1. Concentric situated at the horizontal central (y–z) plane of the cavity. In this case (a thin disk or a shell), the displacement part of the integral [A7] can be ignored and

$$I_{pp}(\mathrm{cd}) \propto \int_0^{\mathrm{cd}/2} \int_0^{2\pi} \times \sqrt{4\rho^2 \cos(2\phi) + \sqrt{b^4 - 16\rho^4 \sin^2(2\phi)}}\ \rho d\rho\ d\phi. \quad [A9]$$

Except for certain special cases, the above integral cannot be solved analytically and must be computed numerically. Again, $e = 2\rho$. The restriction cd $\leq b$ expresses that the maximal available cd of the circular sample is limited by the width of the cavity, b. Because of the symmetry of the integral over ϕ, it need only be integrated over the first quadrant and then multiplied by four.

2.2. Movement of the circular sample along the central cavity x axis. For a circular sample displaced a distance $x \in \langle -a/2, a/2\rangle$ from the cavity center, Eq. [A9] must be multiplied by a factor of $G(x)$, Eq. [A5], giving

$$I_{pp}(cd) \propto \sin^2\left(\frac{\pi}{a}\left(x + \frac{a}{2}\right)\right) \int_0^{cd/2} \int_0^{2\pi} \times \sqrt{4\rho^2\cos(2\phi) + \sqrt{b^4 - 16\rho^4\sin^2(2\phi)}}\ \rho d\rho\ d\phi. \quad [A10]$$

Note: Again here, the double integral in Eq. [A10] has a constant value during the movement of the circular sample along the cavity x axis, because the sample diameter, cd, remains unchanged.

In the case of a real circular sample (with $L \neq 0$), Eq. [A8], which is valid for the cylindrical sample, must be used.

3. Linelike Sample of Length L and i.d. → 0 Situated on (Moved along) the Central Cavity x Axis

In this case (a thin sample tube or a capillary), the angular function has $D_{\infty h}$ (circular) symmetry and consequently for the X-band cavity is

$$I_{pp}(L_2, L_1) \propto \int_{L_1}^{L_2} \frac{q_0\cos^3\left(\pi \frac{x}{a}\right)}{\sqrt{1 + q_0^2\cos^2\left(\pi \frac{x}{a}\right)}}\, dx, \quad [A11]$$

which is identical to Eq. [6] in Ref. (*12*), where also the movement of linelike sample along the common cavity–sample x axis is precisely analyzed.

This equation well approximates likewise the signal intensity of a thin cylindrical sample of i.d. less than 1.5 mm. See Refs. (*10*), (*12*), and (*13*) for further details. Note: It is assumed that both the microwave field and the modulation field are uniform in the horizontal (y–z) planes of the cavity within a small circular area of the cross section of the thin cylindrical sample.

4. Pointlike Sample of i.d. → 0 and L → 0

4.1. Situated at the horizontal central (y–z) plane of the cavity. In this case, the EPR signal intensity of a pointlike sample situated at any point P(ρ, ϕ, 0) of the central cavity (y–z) plane is expressed directly by Eq. [A1], in which the substitution $e = 2\rho$ is made:

$$I_{pp} \propto \sqrt{4\rho^2\cos(2\phi) + \sqrt{b^4 - 16\rho^4\sin^2(2\phi)}}, \quad [A12]$$

with the restriction $\rho \leq b/2$. See Part I of this Appendix for more information.

4.2. Situated at any point P(ρ, ϕ, x) within the prescribed part of the cavity. In this case, Eq. [A12] must be multiplied by a factor of $G(x)$, Eq. [A5], giving

$$I_{pp} \propto \sin^2\left(\frac{\pi}{a}\left(x + \frac{a}{2}\right)\right) \times \sqrt{4\rho^2\cos(2\phi) + \sqrt{b^4 - 16\rho^4\sin^2(2\phi)}}, \quad [A13]$$

again with the restrictions $\rho \leq b/2$ for the angular part and $x \in \langle -a/2,\ a/2\rangle$ for the linear part. Note: For a pointlike sample situated on the cavity x axis, P(0, 0, x), the angular function is equal to b, and the above equation is simplified to a sine-squared function, Eq. [A5].

5. A Real Pointlike Sample of i.d. ≠ 0 and L ≠ 0

5.1. Situated at the horizontal central (y–z) plane of the cavity. As was shown in Part I of this Appendix, the correction to the real shape of a pointlike sample (with i.d. ≠ 0) can be introduced by the substitution $e = 2\rho$ + i.d. in Eq. [A1], giving

$$I_{pp} \propto \sqrt{(2\rho + \text{i.d.})^2\cos(2\phi) + \sqrt{b^4 - (2\rho + \text{i.d.})^4\sin^2(2\phi)}}, \quad [A14]$$

with the restriction $\rho \leq (b - \text{i.d.})/2 - L_W$ for the sample rotation radius at the cavity (y–z) plane.

5.2. Situated at any point P(ρ, ϕ, x) within the prescribed part of the cavity. In this case, Eq. [A14] must be multiplied by Eq. [A11], which describes the linelike sample (because $L \neq 0$ for a real pointlike sample), giving

$$I_{pp} \propto \int_{L_1}^{L_2} \frac{q_0\cos^3\left(\pi \frac{x}{a}\right)}{\sqrt{1 + q_0^2\cos^2\left(\frac{x}{a}\right)}}\, dx \times \sqrt{(2\rho + \text{i.d.})^2\cos(2\phi) + \sqrt{b^4 - (2\rho + \text{i.d.})^4\sin^2(2\phi)}}, \quad [A15]$$

with the additional restriction cc $\in \langle -(a + L)/2, (a + L)/2\rangle$ for the sample movement along the cavity x axis. Note: The integral from a linear part has a constant value during the sample rotation at the given (y–z) plane, because the x coordinate of the sample center remains constant.

Equation [A15] well approximates likewise the signal intensity of the thin cylindrical sample of length L and i.d. less than 1.5 mm, which is situated parallel with the central cavity x axis. The center of the sample, $S_c(0, 0, *L/2)$, can be situated at any point $P_c(\rho, \phi, x)$ within the prescribed part of the microwave cavity. Again here, $\rho \leq (b - \text{i.d.})/2 - L_W$.

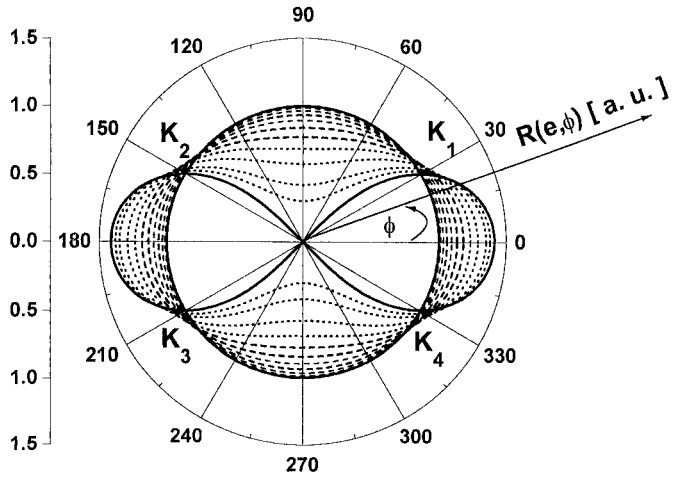

FIG. 10. General shape of the Cassinian curves, $R(e, \phi)$, in the polar coordinate system, Eq. [B2], calculated for $b = 11$, $\phi \in \langle 0, 2\pi \rangle$, and $e = 0$ (a "basic circle" (solid line)), $e \in \langle 1, 7 \rangle$ (an oval (dashed lines)), $e \in \langle 8, 10.5 \rangle$ (a figure eight (dotted lines)), and $e = b$ (a Bernoulli lemniscate (bold solid line)). $e \cong 7.8$ for the boundary oval. The function value of the basic circle, which is independent of the rotation angle, ϕ, was taken as unity. For further details, see text.

APPENDIX B

Definition and Properties of the Cassinian Curves

Let the points F_1 and F_2 be the foci and the line segment $F_1F_2 = 2e$ be the foci length. A Cassinian curve is defined as the locus of points M for which the product $MF_1 \cdot MF_2$ of the distances to the ends of a given segment F_1F_2 is equal to the square of the given segment b, $MF_1 \cdot MF_2 = b^2$. The midpoint, O, of the segment F_1F_2 is called the center of the Cassinian curve. The points A_1, A_2, B_1, and B_2 are the vertices, and the segments $A_1A_2 = 2\alpha$ and $B_1B_2 = 2\beta$ are called the major and minor axes of the Cassinian curve, respectively ($\alpha \geq 0$, $\beta \geq 0$). For further details, see elsewhere (*31*, *32*).

In polar coordinates, $\{R, \phi\}$, with O as the pole and OX as the polar axis, the Cassinian curves can be shown to be

$$R^4 - 2e^2R^2\cos(2\phi) + e^4 - b^4 = 0, \qquad [B1]$$

or

$$R^2 = e^2\cos(2\phi) \pm \sqrt{b^4 - e^4\sin^2(2\phi)}. \qquad [B2]$$

In the present work, the EPR signal intensity, I_{pp} (≥ 0), is associated with R (only nonnegative values are taken), the width of the microwave cavity with b, and the radial displacement of a pointlike sample from the origin with e. The general shape of the Cassinian curves calculated using parameters applicable to the Bruker TE_{102} and TE_{104} rectangular cavities ($b = 11$ mm, $e \in \langle 0, b \rangle$, and $\phi \in \langle 0, 2\pi \rangle$) is illustrated in Fig. 10. Since $b^4 \geq e^4$, only the plus sign is taken, and Eq. [B2] gives always a real and closed curve, which varies in shape from circular ($R^2 = b^2$) at $e = 0$ (solid line), through oval at $0 < e < b/\sqrt{2}$ (dashed lines), to figure eight at $b/\sqrt{2} < e < b$ (dotted lines). The curve corresponding to $e = b/\sqrt{2}$ ($\cong 7.8$ mm) is termed the boundary oval and if $e = b$ the Cassinian curve reduces to the Bernoulli lemniscate (bold solid line). It is clear that all curves are axially symmetric with respect to the major and minor axes and, hence, with respect to the center, O, and intersect at four points, $K_1(\phi = 30°)$, $K_2(\phi = 150°)$, $K_3(\phi = 210°)$, and $K_4(\phi = 330°)$, whose distance from the center, O, is $\cong b$. It is valid that $\alpha \geq \beta$ and $\alpha \geq e$ and that $\alpha \in \langle b, b\sqrt{2} \rangle$ and $\beta \in \langle 0, b \rangle$. The ratios $\kappa = \beta/\alpha$ and $\epsilon = e/\alpha$ are called the coefficient of compression and the eccentricity of the Cassinian curve, respectively ($0 \leq \kappa \leq 1$, $0 \leq \epsilon \leq 1$, and $\epsilon = 1 - \kappa$). Note: For a basic circle, $\kappa = 1$ and $\epsilon = 0$; for the Bernoulli lemniscate, $\kappa = 0$ and $\epsilon = 1$.

ACKNOWLEDGMENTS

This work was supported by The British Council, Slovakia, and the Slovak Grant Agency for Science. We are grateful to Dr. V. Nagy, Dr. J. Plaček, and Professor A. Staško for fruitful discussions during the course of this work.

REFERENCES

1. C. P. Poole, *in* "Electron Spin Resonance: A Comprehensive Treatise on Experimental Techniques," pp. 257–339, Wiley-Interscience, New York (1967).
2. G. Casteleijn, J. J. ten Bosch, and J. Smidt, *Appl. Phys.* **39,** 4375 (1968).
3. C. Mailer, T. Sarna, H. M. Swartz, and J. S. Hyde, *J. Magn. Reson.* **25,** 205 (1977).
4. D. P. Dalal, S. S. Eaton, and G. R. Eaton, *J. Magn. Reson.* **44,** 415 (1981).
5. M. Sueki, G. A. Rinard, S. S. Eaton, and G. R. Eaton, *J. Magn. Reson., Ser. A* **118,** 173 (1996).
6. V. J. Nagy and J. Plaček, *Fresenius' J. Anal. Chem.* **343,** 863 (1992).
7. R. C. Barklie and L. Sealy, *J. Magn. Reson.* **97,** 611 (1992).
8. M. Mazúr, M. Valko, R. Klement, and H. Morris, *Anal. Chim. Acta* **333,** 249 (1996).
9. M. Mazúr, M. Valko, H. Morris, and R. Klement, *Anal. Chim. Acta* **333,** 253 (1996).
10. M. Mazúr, H. Morris, and M. Valko, *J. Magn. Reson.* **129,** 188 (1997).
11. M. Mazúr, M. Valko, and P. Pelikán, *Chem. Papers* **51,** 134 (1997).
12. M. Mazúr, M. Valko, and H. Morris, *Anal. Chim. Acta* **367,** 233 (1998).
13. M. Mazúr, M. Valko, M. Micov, and H. Morris, *Anal. Chim. Acta* **373,** 107 (1998).
14. M. L. Randolph, Quantitative considerations in electron spin resonance studies of biological materials, *in* "Biological Applications of Electron Spin Resonance" (H. M. Swartz, J. R. Bolton, and D. C. Borg, Eds.), pp. 119–153, Wiley-Interscience, New York (1972).
15. V. Nagy, *Appl. Magn. Reson.* **6,** 256 (1994).
16. ER Series User's Manual, Bruker Analytical Messtechnik Gmbh, EPR Division (1983).
17. E-4 EPR spectrometer system, Technical manual, Varian Analytical Instrument Division, No. 87-125-001 (1971).

18. M. Mazúr, M. Valko, and H. Morris, *Rev. Sci. Instrum.* **68,** 2514 (1997).

19. A. Abragam and B. Bleaney, "Electron Paramagnetic Resonance of Transition Ions," Oxford Univ. Press, London (1970).

20. C. P. Poole, Jr., and H. A. Farach, *in* "Theory of Magnetic Resonance," pp. 46–79, Wiley-Interscience, New York (1987).

21. J. A. Weil, J. R. Bolton, and J. E. Wertz, "Electron Paramagnetic Resonance Spectroscopy, Elementary Theory and Practical Applications," Wiley-Interscience, New York (1994).

22. R. S. Alger, *in* "Electron Paramagnetic Resonance: Techniques and Applications," pp. 200–220, Wiley-Interscience, New York (1968).

23. J. E. Wertz and J. R. Bolton, *in* "Electron Spin Resonance, Elementary Theory and Practical Applications," pp. 131–191, McGraw-Hill, New York (1972).

24. H. M. Swartz, J. R. Bolton, and D. C. Borg, *in* "Biological Applications of Electron Spin Resonance," pp. 483–539, Wiley-Interscience, New York (1972).

25. L. J. Berliner, *in* "Spin Labeling, Theory and Applications I," pp. 454–523, Academic Press, New York (1976).

26. L. J. Berliner, *in* "Spin Labeling, Theory and Applications II," pp. 223–290, Academic Press, New York (1979).

27. P. Pelikán, M. Liška, M. Valko, and M. Mazúr, *J. Magn. Reson.* **122,** 9 (1996).

28. P. F. Knowles, D. Marsch, and H. W. E. Rattle, *in* "Magnetic Resonance of Biomolecules. An Introduction to the Theory and Practice of NMR and EPR in Biological Systems," pp. 168–207, Wiley, London (1976).

29. P. Fajer and D. Marsh, *J. Magn. Reson.* **49,** 212 (1982).

30. R. G. Kooser, W. V. Volland, and J. H. Freed, *J. Chem. Phys.* **50,** 5243 (1969).

31. M. Vygodsky, *in* "Mathematical Handbook, Higher Mathematics," pp. 775–782, Mir, Moscow (1971).

32. H. J. Bartsch, *in* "Mathematische Formeln," pp. 457–458, VEB, Fachbuchverlag, Leipzig (1960).